La Trobe University

Department of Physics

Space Physics Honours Thesis

Enhanced Beam Steering Capability for the TIGER SuperDARN radars

Ryan Healey

December 9, 2005

Supervisor: Dr. Murray L. Parkinson

To increase the field of view of the TIGER (Tasman International Geospace Environment Radar) SuperDARN (Super Dual Auroral Radar Network) radars new phasing boxes have been built at La Trobe University. A box that rotates the field of view of the Bruny Island radar to include Macquarie Island (MQI) was tested using geophysical observations and was found to work. Macquarie Island contains basic space science instruments which can be used to improve the interpretation of TIGER observations. Using the Macquarie Island phasing box a series of campaigns were carried out to gather data for future analysis. One of these campaigns was analysed using the map potential model to determine the 2-D convection pattern. This showed a possible new convection cell in the pre-noon sector sub-auroral ionosphere. A box that shifts the field of view of the Bruny Island radar to include the predicted HAARP (High frequency Active Auroral Research Program) conjugate point was also built. Preliminary tests suggest the HAARP box is working but the data will require further analysis to achieve confidence. A campaign to detect an effect at the HAARP conjugate point was run but no conclusive effect has been obtained so far. Finally a phasing box that will be used to observe F Region scatter with the Unwin radar above E Region scatter observed by the Bruny Island radar is under construction.

Statement of Authorship

Except where reference is made in the text of the thesis, this thesis contains no material published elsewhere or extracted in whole or in part from a thesis presented by me for another degree or diploma.

No other persons work has been used without due acknowledgement in the main text of the thesis.

This thesis has not been submitted for the award of any other degree or diploma in any other tertiary institution.

Ryan Healey

Acknowledgements

Contents

List of Figures

List of Tables

1 Introduction

1.1 SuperDARN and TIGER

SuperDARN (Super Dual Auroral Radar Network) is an international network of coherent backscatter HF[1] radars dedicated to ionospheric research. SuperDARN radars have an approximate field of view of $\approx 52°$ comprised of 16 different beams separated by $3.24°$ and they sample ranges between about 180 km to over 3 000 km usually in 45 km steps [6]. They measure ionospheric motion by Bragg scattering off decametre scale electron density irregularities in the ionosphere [6].

Ionospheric irregularities tend to be field aligned which means that for a backscattered signal to be returned to the radar the radio waves must become orthogonal to the magnetic field lines which at high latitudes are nearly vertical [6]. A HF radar can take advantage of ionospheric propagation to refract the radio waves to orthogonality with the magnetic field for F Region heights at high latitude [6].

TIGER (Tasman International Geospace Environment Radar) consists of two radars operated by La Trobe University [5] and is a component of SuperDARN [5, 11]. Both components of TIGER are at a lower latitude than other SuperDARN radars, except for the recently commissioned Wallops Island radar, allowing the TIGER radars to observe the auroral oval during disturbed geomagnetic conditions when the zone of intense auroral irregularities expands too far equatorward for the rest of the SuperDARN network to observe.

---

[1]High Frequency spans the range of 3 MHz to 30 MHz. SuperDARN radars work over the range of 8 MHz to 20 MHz

The Tasmanian Component of TIGER (Figure 1.1) is located on Bruny Island (43.38° S, 147.23° E) and points toward geographic south to scan opposite the field of view of the Halley radar located in Antarctica.

Figure 1.1: The TIGER Bruny Island radar viewed from behind. The 4 antenna interferometer array is shown in the foreground and the 16 antenna main array in the background.

The TIGER Unwin radar (Figure 1.2) near Invercargill, New Zealand (46.51° S, 168.37° E) was added in 2004 and has a field of view which overlaps that of the TIGER Bruny Island radar, both of which are shown in Figure 1.3. This allows the line of sight velocity vectors of each radar to be combined to generate two dimensional convection maps of the ionosphere.

The method used to rotate the field of view of these radars from the default boresights described in this thesis provides the opportunity for some novel experiments.

Figure 1.2: The TIGER Unwin radar viewed from the front. The 16 antenna main array is shown in the foreground and the 4 antenna interferometer array in the background.

1.2 Map Potential Model

Whilst merging the line of sight vectors from two or more radars allows for the determination of two dimensional velocity vectors, this can only work when both radars have determined a line of sight velocity vector in the same spatial region. This is usually only a subset of the line of sight vectors observed by both radars.

Ionospheric winds at high latitudes tend to flow along lines of electric isopotential[2] due to $\underline{E} \times \underline{B}$ drift [12]. The map potential analysis developed by Ruohoniemi et al. uses SuperDARN line of sight velocities to model the electric potentials using fitted 2D velocity vectors [12, 13]. A statistical model is used to model the electric potential in regions not constrained by data [12, 13].

---

[2]These are analogous to isobars in the lower atmosphere
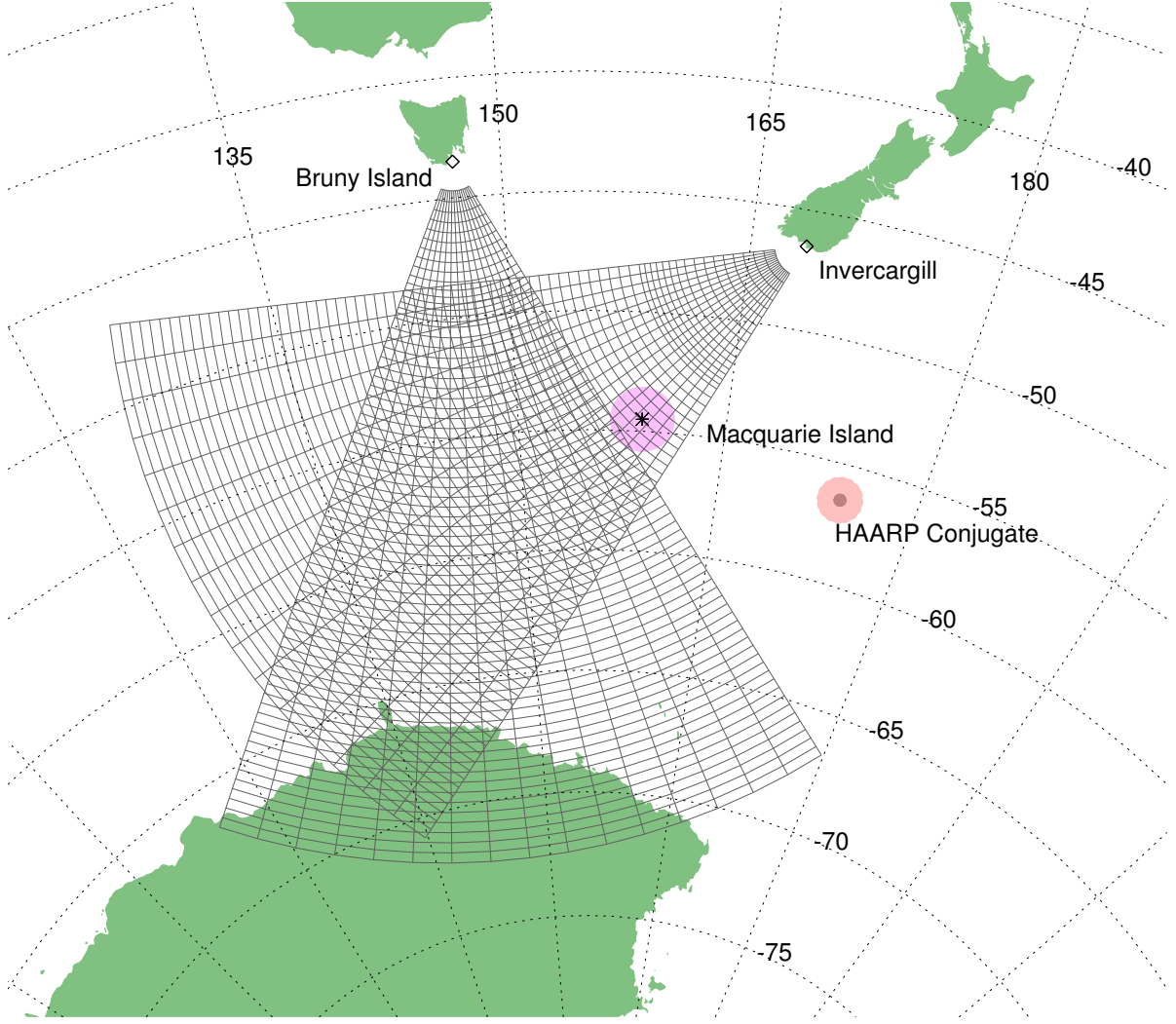
Figure 1.3: The default fields of view of the TIGER radar pair. Each field of view is divided into sixteen beams with the western most beam numbered 0 and the eastern most beam numbered 15. The standard 45 km range gates are also shown.

The electrostatic potential Φ obtained from $\underset{\sim}{E} = -\nabla\Phi$ is expanded using spherical harmonic functions as:

$$\Phi(\theta, \phi) = \sum_{\ell=0}^{L} \sum_{m=-M}^{M} A_{\ell m} Y_{\ell m}(\theta, \phi) \tag{1.1}$$

where $A_{\ell m}$ is a complex coefficient, $Y_{\ell m}$ is a spherical harmonic function of order ℓ and degree m, ϕ is the longitude and θ is the colatitude. In the electrostatic case the analysis

is actually done with a purely real Φ and so an equation of the form:

$$\Phi(\theta, \phi) = \sum_{\ell=0}^{L} A_{\ell 0} P_{\ell}^{0}(\cos\theta) + \sum_{m=1}^{\ell} \left(A_{\ell m}\cos m\phi + B_{\ell m}\sin m\phi\right) P_{\ell}^{m}(\cos\theta) \qquad (1.2)$$

is used with $A_{\ell m}$ and $B_{\ell m}$ both real and P_{ℓ}^{m} are the associated Legendre functions.

The convection pattern is then fitted by taking line of sight velocity vectors and minimising:

$$\chi^2 = \sum_{i=1}^{N} \frac{1}{\sigma_i^2} \left[\underset{\sim}{v_i} \bullet \underset{\sim}{\hat{k}_i} - w_i\right]^2 \qquad (1.3)$$

where v_i is the fitted velocity vector at point i, w_i is the line of sight velocity at point i, $\hat{k}_i$ is the unit vector in the direction of the radar line of sight and σ_i is the uncertainty of the line of sight velocity. Once $\underset{\sim}{v}$ has been found $\underset{\approx}{E}$ can be found since:

$$\underset{\sim}{v} = \frac{\underset{\approx}{E} \times \underset{\approx}{B}}{B^2} \qquad (1.4)$$

The electric field and hence the electric potential are implied by the fitted velocity vectors.

The enhanced beam steering capability described in this thesis provides the opportunity to extend the map potential analysis to new spatial regions.

1.3 Magnetic Conjugacy

Magnetic conjugate points are two points on the Earth's surface or at a height above the Earth's surface which are connected by a single magnetic field line [1]. The magnetic field lines tend to be equipotential because electrons and ions have a high mobility along magnetic field lines compared to mobility perpendicular to magnetic field lines [1].

Conjugate points tend to move around because of external magnetospheric currents associated with the global substorm cycle. This is particularly the case above 60° magnetic [1].

1.4 Macquarie Island

Macquarie Island is a sub-antarctic island situated approximately 1 500 km south east of Tasmania. It is 34 km long and 5 km wide at its widest point [4]. There is an Australian Antarctic Division station located at the northern end of the Island [4] as shown in Figure 1.4. Basic space science instruments including magnetometers, an auroral imager, a digital ionosonde and a riometer are located on Macquarie Island [10].

Macquarie Island is the only land mass that is near the field of view of the TIGER Bruny Island radar[3] as well as being in the field of view of the Unwin radar.

Hardware modifications have been made to the Bruny Island radar which allow the radar field of view to be rotated to place beam 14 above Macquarie Island, thereby allowing for 2D velocity vector determinations for comparison with measurements made with other instruments located on Macquarie Island.

1.5 Ionospheric Heaters

Ionospheric heaters are large radio transmitters that heat the ionosphere by emitting radio waves that are absorbed in a narrow layer of the ionosphere [3]. HF radio waves are used since they are absorbed in a narrow range of heights [3] by transmitting at the plasma frequency of the desired height range [3]. An increase in electron temperature is also centered around a narrow range of heights [3, 16].

To be able to heat the ionosphere located one hundred kilometres or more above the Earth a large amount of power must be emitted which results in ionospheric heaters being expensive to operate [3]. Despite the high cost of both construction and operation of ionospheric heaters many have been built. The potential scientific returns derived from controlled studies of the ionosphere are immense.

---

[3]This is not strictly true. Antarctica is located within the TIGER Bruny Island field of view but at an extreme range where the radar measurements are unreliable because of lower power at extreme range and bad lags in the auto correlation functions
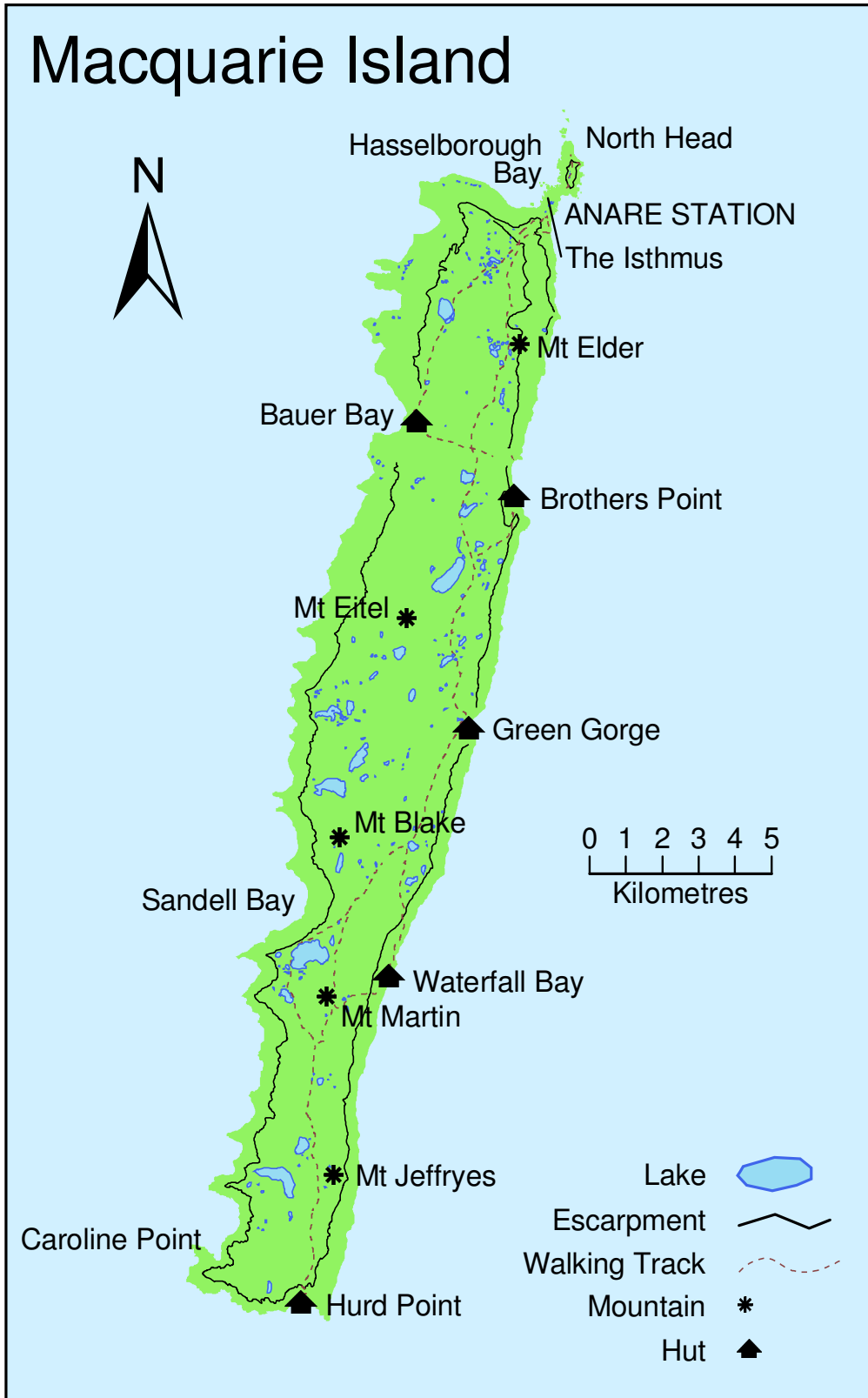
Figure 1.4: Macquarie Island [2]

An ionospheric heater is usually a phased array of crossed dipole antennas which allows for the production of circularly polarised radiation. The HAARP (High frequency Active Auroral Research Program), (Figure 1.5), SPEAR (Space Plasma Exploration by Active Radar) and EISCAT (European Incoherent Scatter) Tromsø heaters, for example, are of this design.

Figure 1.5: The HAARP Ionospheric Heater near Gakona, Alaska. The phased array crossed dipole antennas are clearly visible. From: `http://www.haarp.alaska.edu`

Ionospheric heaters change the propagation of radio waves passing through the heated region [3, 15] by changing the electron density and temperature. This effect was first noticed in the 1930's and is called the Luxembourg effect after the power station at Luxembourg that was modulating signals from a Swiss station received in Holland [3].

Airglow is also modified by ionospheric heating [3, 14] but there is considerable variation depending on the auroral electron parameters [14]. Most airglow modification tends to occur during F-region heating with airglow from E-region heating being rather rare [7, 14]. Airglow produced by ionospheric heaters is usually too faint to be visible to the naked eye and detection requires low light cameras [7, 14]. However HAARP has recently produced modulation of an existing aurora that was visible to the naked eye [7].

15

Ionospheric heating can also affect the conductivity of the ionosphere [3, 16]. This can allow a heater beam with a low frequency modulation to create an antenna in the ionosphere which transmits at the frequency of the modulation [3, 16]. ULF waves have a higher amplitude due to the electron density being modulated whereas at ELF and VLF only the electron temperature is modulated and thus mostly the electron Pedersen conductivity which is a relatively small component of the conductivity is modulated [16].

Artificial scatter associated with ionospheric heating tends to be of very low spectral width when observed by SuperDARN radars [9] due to artificial scatter being of high coherency and lifetime compared to natural scatter [9].

The HAARP conjugate point is located to the east of the default TIGER radar field of view.

2 Phasing Boxes

To rotate the field of view of a SuperDARN radar a phasing box was designed at La Trobe University to change the phasing of the antenna array and thereby steer the array.

2.1 SuperDARN Radar Beam Steering

SuperDARN radars are HF phased array radars which operate over a broad frequency range (8 MHz to 20 MHz) [8].

To steer a phased array the signal to each antenna is given a phase shift:

$$\phi = 2\pi \frac{x}{\lambda} \tag{2.1}$$

Figure 2.1 shows that for a linear antenna array such as that used by a SuperDARN radar (2.1) becomes:

$$\phi = 2\pi \frac{d\sin(\theta)}{\lambda} \tag{2.2}$$

Replacing the wavelength with the frequency gives:

$$\phi = 2\pi \frac{\nu}{c} d\sin(\theta) \tag{2.3}$$

Where (2.3) can be expressed as a time delay:

$$t_d = \frac{d\sin(\theta)}{c} \tag{2.4}$$

Note that this time delay is independent of frequency, so the antenna array can be steered to the same direction at all frequencies, using the same set of time delays.
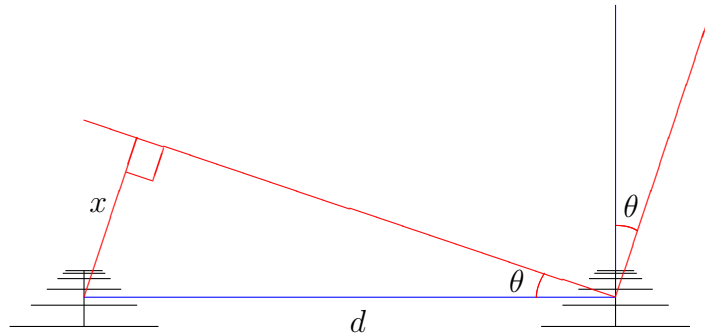
Figure 2.1: A simplified representation of a phased array. d is the separation between two elements in the phased array, θ is the desired amount of beam steering, x is the displacement in the direction of the desired beam that would be needed to steer the beam if the array were to be physically rotated. Steering a phased array electronically is accomplished by imitating this extra 'distance' for each antenna in the array relative to the one at the end in which the array is to be 'turned'.

With SuperDARN radars, beam steering is performed using a phasing matrix (bottom of Figure 2.2) which selects the correct combination of time delays to produce 16 beams separated by 3.24° in azimuth over a field of view of ≈ 52° [8]. This thesis describes an additional phasing box (Figures 2.2 and 2.3) used to rotate the field of view of the radar. A phasing box is a small device using Data Delay Devices 1513 fixed passive delay lines to add additional delays to the signal that goes to each antenna, thereby providing additional beam steering to that provided by the phasing matrix.

2.2 Antenna Pattern Calculations

SuperDARN radars produce a main beam that depending on frequency is 2.5° to 6° wide [8]. However sidelobes are a problem with most antenna arrays.

Since the sidelobes from a phased array tend to get progressively worse the further away the main beam is steered from the boresight of the array, it is necessary to calculate

Figure 2.2: The black box labeled 'TIGER PHASING DELAY' is the Macquarie Island phasing box. The phasing matrix is below the phasing box and the BASbox which performs radar control functions is above the phasing box. Photograph courtesy Mark Gentile.

the radiation pattern from the array if one is to know whether it is even worth adding additional beam steering.

Sidelobes tolerable if they are small enough compared to the mainlobe that the contribution to the signal from the sidelobe is small. For this purpose the `arraypattern` program was written to calculate the 2D azimuthal radiation pattern of a SuperDARN radar.

2.2.1 Calculation of Phased Array Radiation Patterns

The array factor was calculated by taking values of the radiation intensity in a circle around the centre of the array with a 100 km radius to ensure the calculations were applicable to the far field of the radar.
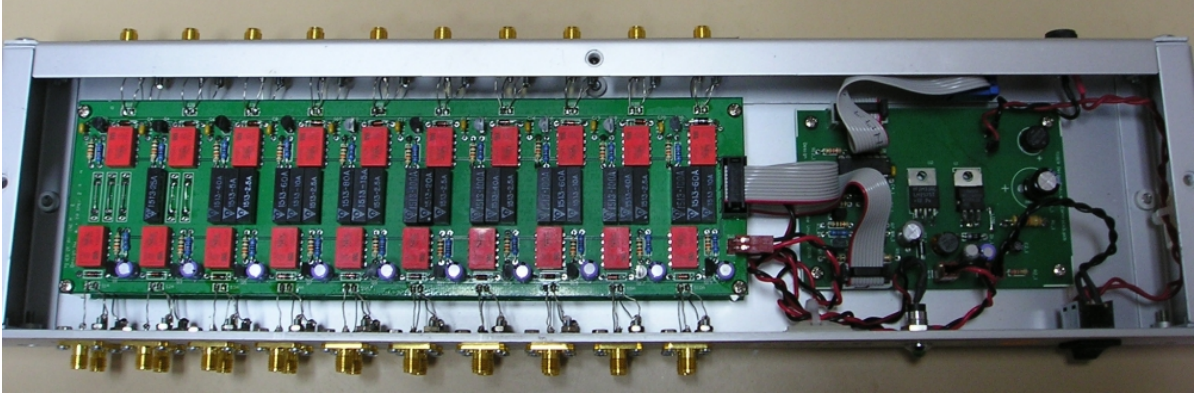
Figure 2.3: The inside of the HAARP phasing box. The stacked circuit boards on the left contain the time delays (black chips) and the relays (red chips). The control board on the right receives the control signals from the BASbox and sets the relays to either pass the signal through the delay lines or bypass them. Photograph courtesy Mark Gentile.

First the phaselength was calculated as:

$$\ell_\phi = \frac{2\pi}{\lambda}\left(D + ct_d\right) \tag{2.5}$$

where λ is the wavelength of the emitted radiation, D is the distance of the point from the antenna and t_d is the time delay being applied to the antenna the phaselength is being calculated for.

The phase length was then converted to a complex phasor by:

$$\varphi = \cos(\ell_\phi) + i\sin(\ell_\phi) \tag{2.6}$$

The amplitude of the radiation was then computed by summing all 16 phasors and then computing the magnitude of the total phasor. This was repeated for all azimuthal angles around the array in steps of one degrees.

To model the array factor for a particular beam number the program used (2.4) to compute the required time delays for each antenna with the additional time delays that a phasing box provided included in the program as an array.

The one way power was calculated by squaring the total amplitude and the two way power calculated by raising the amplitude to the fourth power[1].

2.2.2 Approximation of Sabre 608 Antenna Pattern

SuperDARN radars, with the exception of the new Wallops Island radar[2], use Sabre Communications Model 608 Log Periodic antennas in the phased arrays. The radiation pattern of the array is the array factor calculated previously multiplied by the pattern of the antennas used. The Sabre 608 antenna pattern was approximated by a cosine squared distribution around the antenna with a factor to account for the forward directivity.

The backlobe of the Sabre 608 antenna has a power loss (in dB) relative to the main lobe that is about the same as the transmitted frequency (in MHz) so the front to back ratio was approximated as:

$$R_{f \to b} = 10^{f/10000} \tag{2.7}$$

where f is the frequency in kilohertz (as are entered into `arraypattern`) and the amplitude loss was then obtained by taking the square root of (2.7).

2.3 Beam Steering with the MQI Phasing Box

To steer beam 14 above Macquarie Island a rotation of the radar boresight of 9.3° is needed. A phasing box was built to rotate the field of view of the TIGER Bruny Island radar 9.3° to the East to allow TIGER measurements to be compared with those made with instruments on the island.

The antenna patterns calculated when the Macquarie Island phasing box is in use do show problematic sidelobes on the eastern most beams at 14 MHz (see Figure 2.5) which are not present without the phasing box until about 16 MHz. This requires that campaigns with this phasing box be restricted to frequencies of less than about 12 MHz.

---

[1]This is equivalent to squaring the one way power
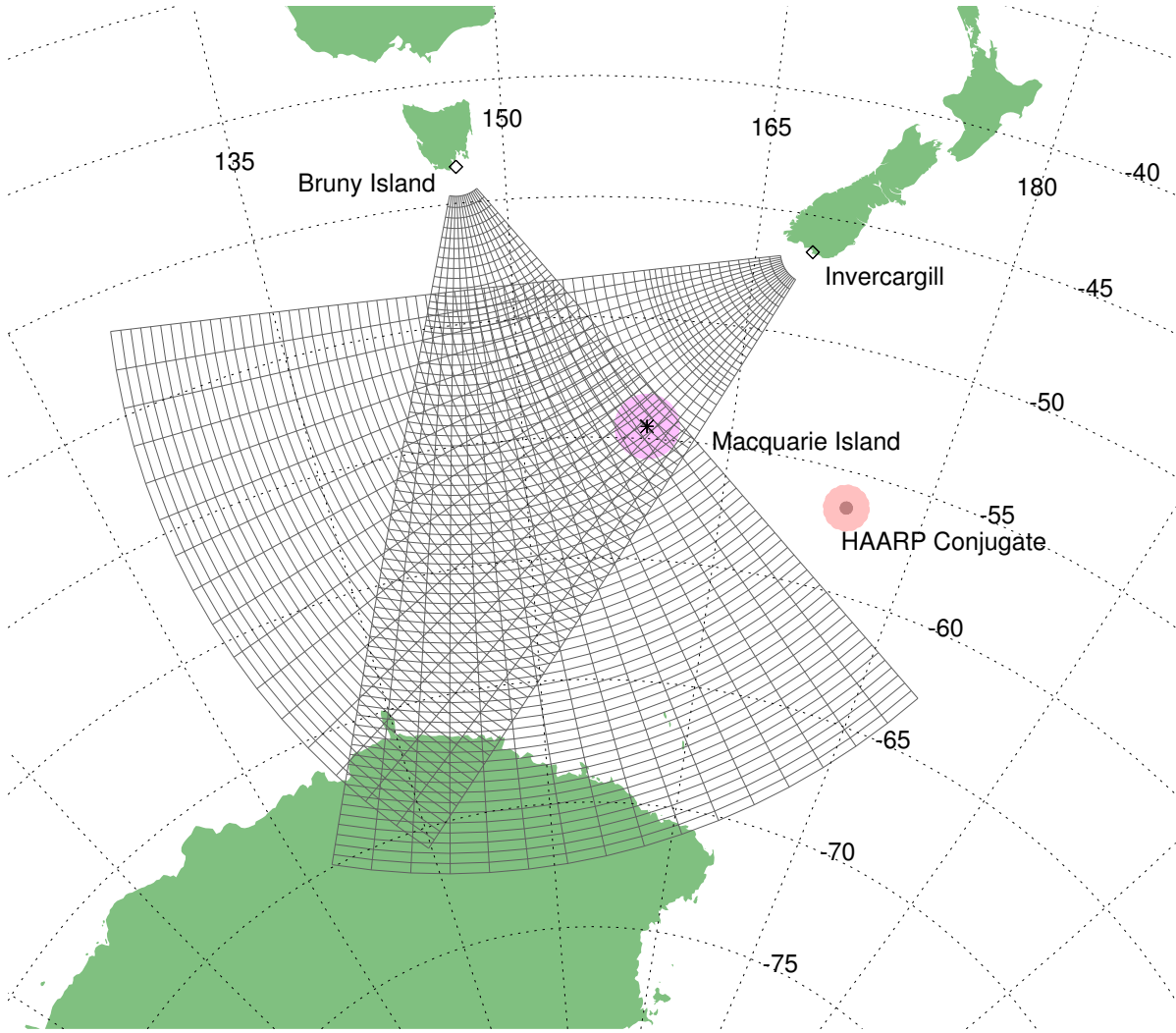[2]The new antenna design has similar performance but is considerably cheaper

Figure 2.4: The radar fields of view when the Macquarie Island phasing box is in use. Notice that beam 14 of the Bruny Island radar now passes over Macquarie Island. The purple circle is an approximate field of view of some of the instruments on the island.
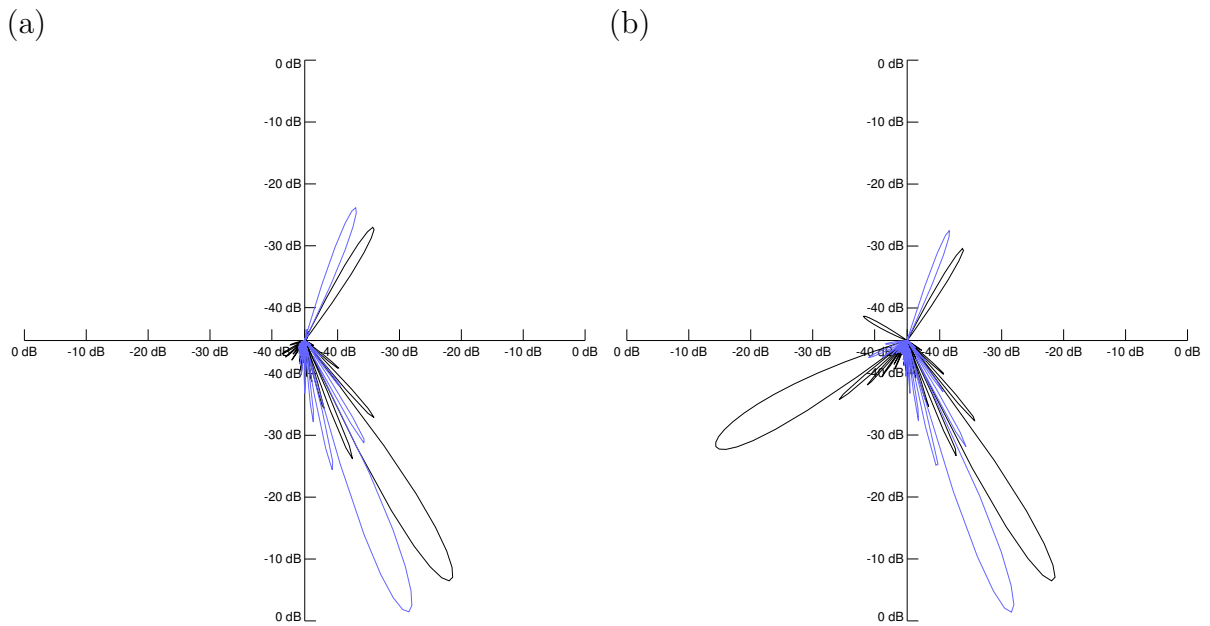
(a)

(b)

Figure 2.5: The radiation patterns for beam 14 (Macquarie Island beam) of the Bruny Island radar with the Macquarie Island phasing box in use (black) and not in use (blue) . (a) is the radiation pattern at 12 MHz where the side lobes are not problematic while (b) is the radiation pattern at 14 MHz where a sidelobe become a problem with the phasing box in use.

2.4 Beam Steering to the HAARP Conjugate Point

For TIGER Bruny Island to detect an inter-hemispheric effect at the HAARP conjugate point a much greater rotation of 28.5° is required to place beam 12 through the HAARP conjugate point. As can be seen in Figure 2.7, this places even more severe limitations on the operating frequency due to the fact that the sidelobes show up at lower frequencies than with the Macquarie Island phasing box.
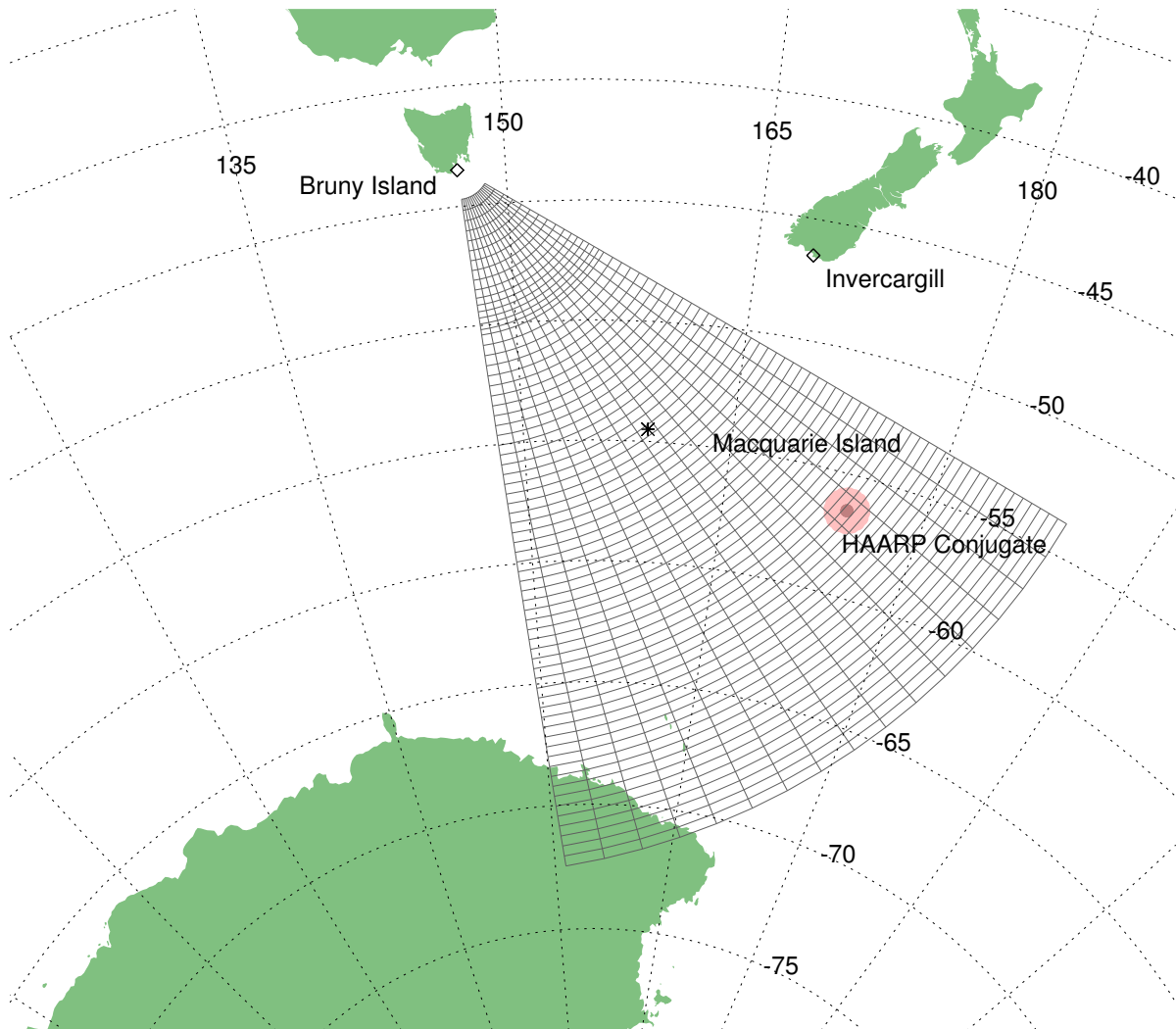
Figure 2.6: Bruny Island radar field of view with the HAARP Phasing Box in use. Note that Beam 12 passes through the HAARP conjugate point. The red areas are located at the HAARP conjugate point and represent the F region heating regions for the full HAARP array at 9.9 MHz (inner) and 2.8 MHz (outer).

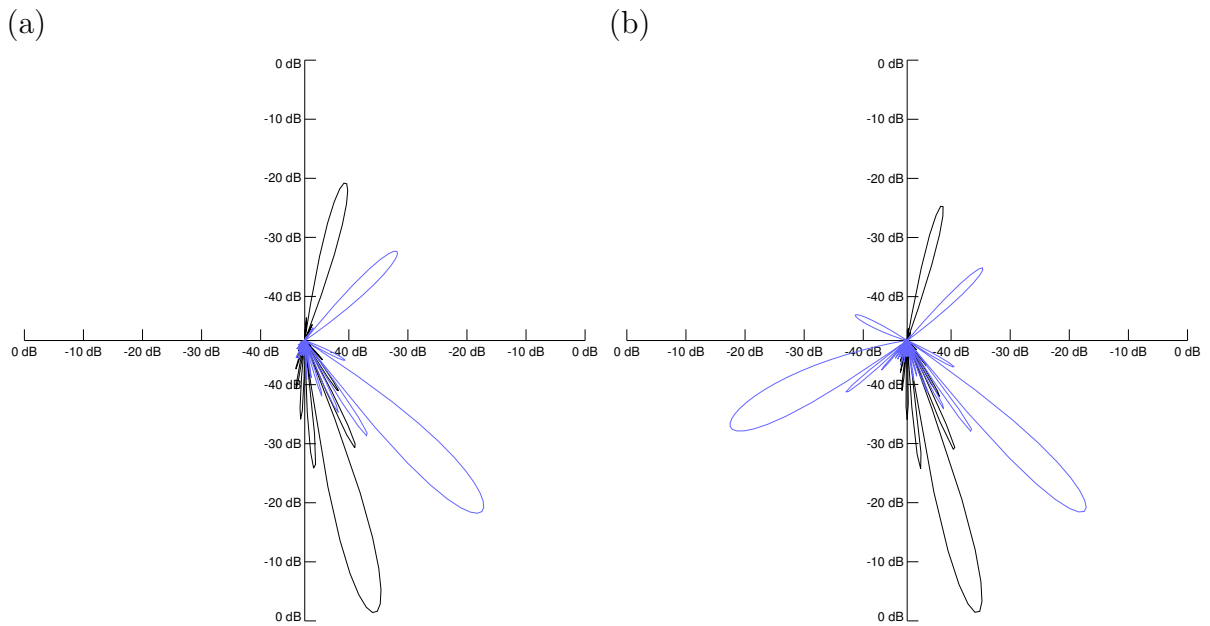(a)   (b)

Figure 2.7: The radiation patterns along beam 12 (which passes through the HAARP conjugate point) of the Bruny Island radar with the HAARP phasing box in use (blue) and not in use (black) . (a) is the radiation pattern at 10 MHz where there are no large sidelobes while (b) is the radiation pattern at 12 MHz where a sidelobe becomes very large.

2.5 Beam Steering to Observe F-region above E-region

SuperDARN radars mostly detect F-region ionospheric scatter but some E-region scatter is detected close in to the radar. If the Unwin radar were rotated by about 4 beams (12.96°) to the north it would be looking at the F-region scatter located directly above the E-region scatter detected at close ranges by the Bruny Island radar. This would allow an investigation of E-region and F-region electrodynamics on the same magnetic field lines.
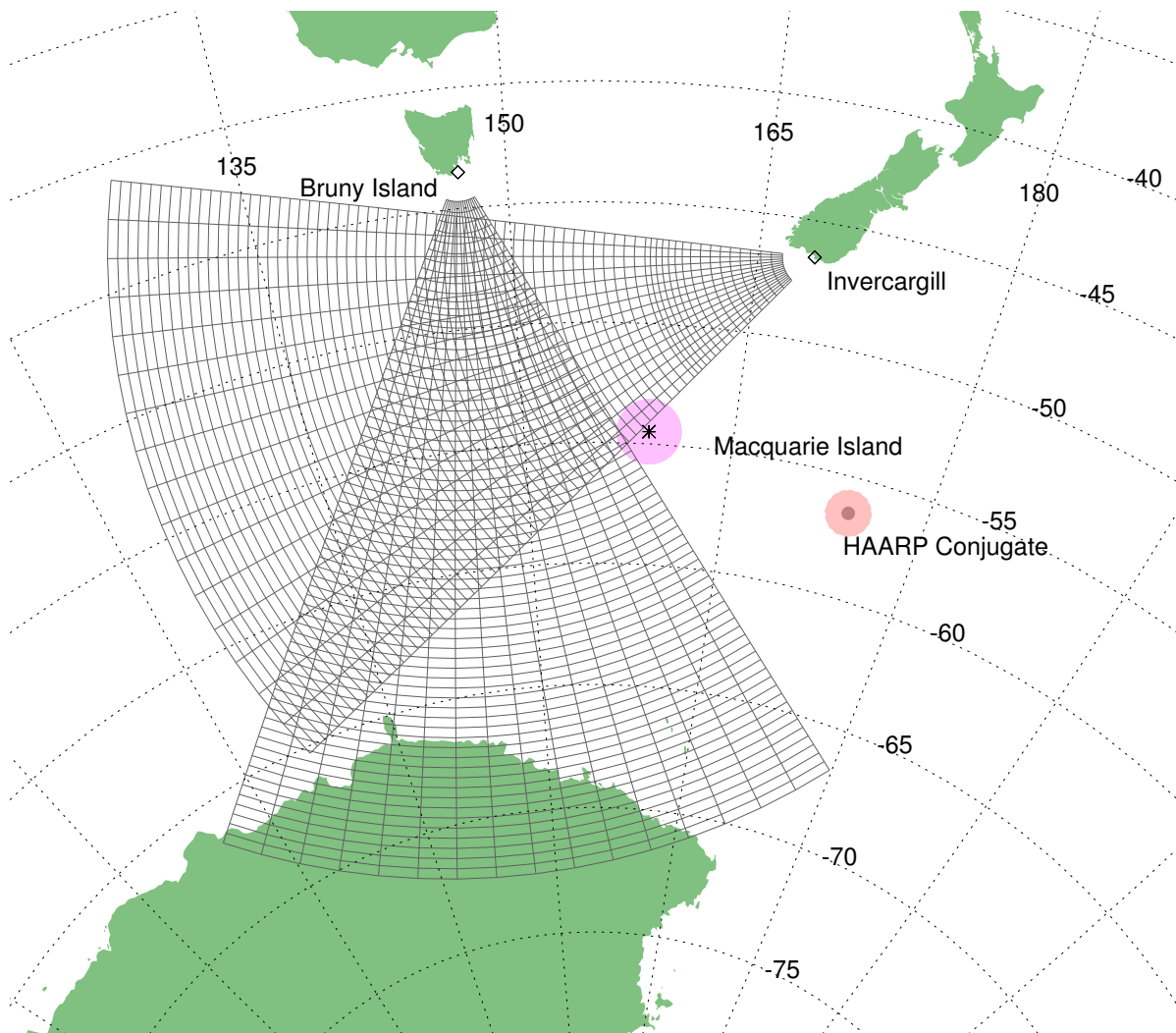
Figure 2.8: Radar fields of view with the E-F Region Phasing Box installed on the Unwin radar. Note that the equatorward beams of the Unwin radar are overlapping the near range gates of the Bruny Island radar where E-region scatter is often observed.

(a)   (b)
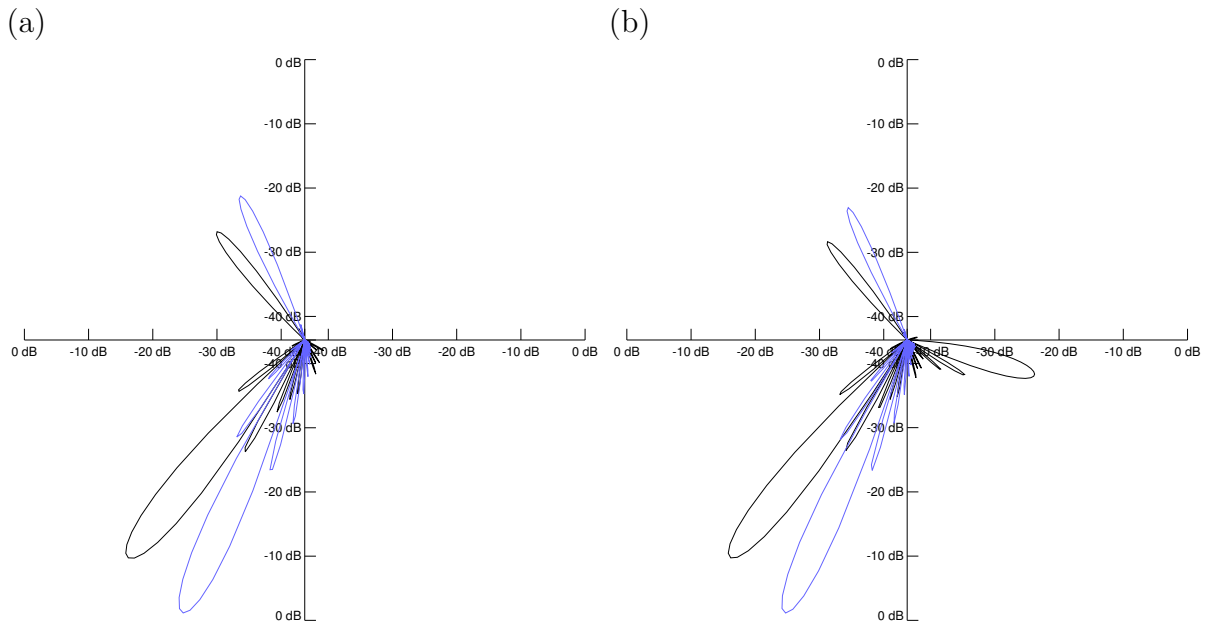
Figure 2.9: The radiation patterns along beam 0 (the beam most degraded by beam steering) of the Unwin radar with the E-F Region phasing box in use (black) and not in use (blue). (a) is the radiation pattern at 11 MHz where there are no noticeable problematic sidelobes while (b) is the radiation pattern at 12 MHz which has a noticeable sidelobe approximately 20 dB down from the main lobe which is considered tolerable. This sidelobe does not show up significantly on any other beams.

27

3 Testing the Phasing Boxes

Testing the phasing boxes was first performed with the `fast_scan` radar control program[1] and a large schedule file that re-ran `fast_scan` with different options every two minutes (specifically, with and without the `-bs` option that turns the phasing box on). This process caused a memory leak that eventually rendered the radar operating system unresponsive.

To remove the limitations of the large schedule file approach for phasing box testing, a new radar control program `pbtest` was modified from `fast_scan`. The wait for minute boundary was removed and the phasing box was switched on and off at the end of each full scan. This caused the phasing box to be switched on and off every 48 s instead of every 2 min, as with the schedule file approach.

Once the data was obtained summary plots were generated and examined for banding that may occur because of field of view switching. The banding can not be used to determine how far the field of view has been rotated but can show whether the phasing box is changing the field of view making it a useful test before further analysis.

After this simple qualitative check a correlation analysis was used on the data to determine how far the field of view was rotated. This was done using the `testphasingbox` program which read the data into memory and separated the data into a set taken with the phasing box off and a set taken with the phasing box on.

---

[1]`fast_scan` performs a scan across the field of view of the radar using a 3 s integration time by default and starting each scan on a minute boundary

These two sets were also sorted by beam number to allow the correlation between the phasing box on and the phasing box off over different beams to be determined. Only points where the radar recorded scatter with the phasing box on and off at the same range gate and in adjacent scans were used. Correlation coefficients were computed for power, velocity, spectral width and the ground scatter flag between different combinations of beams. The correlation should peak when the angular difference between the beams being correlated is approximately the same as the field of view rotation of the phasing box.

3.1 Testing the MQI Phasing Box

A campaign was run on the Bruny Island radar to test the Macquarie Island phasing box on the 14th of March, 2005. The `fast_scan` program was run on the radar with the phasing box switched on and off every two minutes. Enough data was collected during the approximately 14 hour period the radar operated for the phasing box to be fully tested.

The Summary Plots showed strong banding on all beams with 30 such bands visible in one hour which corresponds to a field of view change happening every two minutes. The Summary Plot along beam 8 showed the strongest banding and is shown in Figure 3.1.

The correlation analysis showed a strong peak at an assumed beam shift of 3 beams for most radar parameters (as can be seen in Figure 3.2). The velocity and spectral width did not correlate as well as the power regardless of the assumed field of view rotation. This is most likely due to the velocity fluctuations being of small scale size and high temporal variability whereas the power of the backscattered signal is determined by propagation conditions which are more stable. The ground scatter correlations for velocity and spectral width did not show a clear peak which is likely due to the errors in the measurements of ground scatter are relatively large compared to the velocity and spectral width measurements of ground scatter.
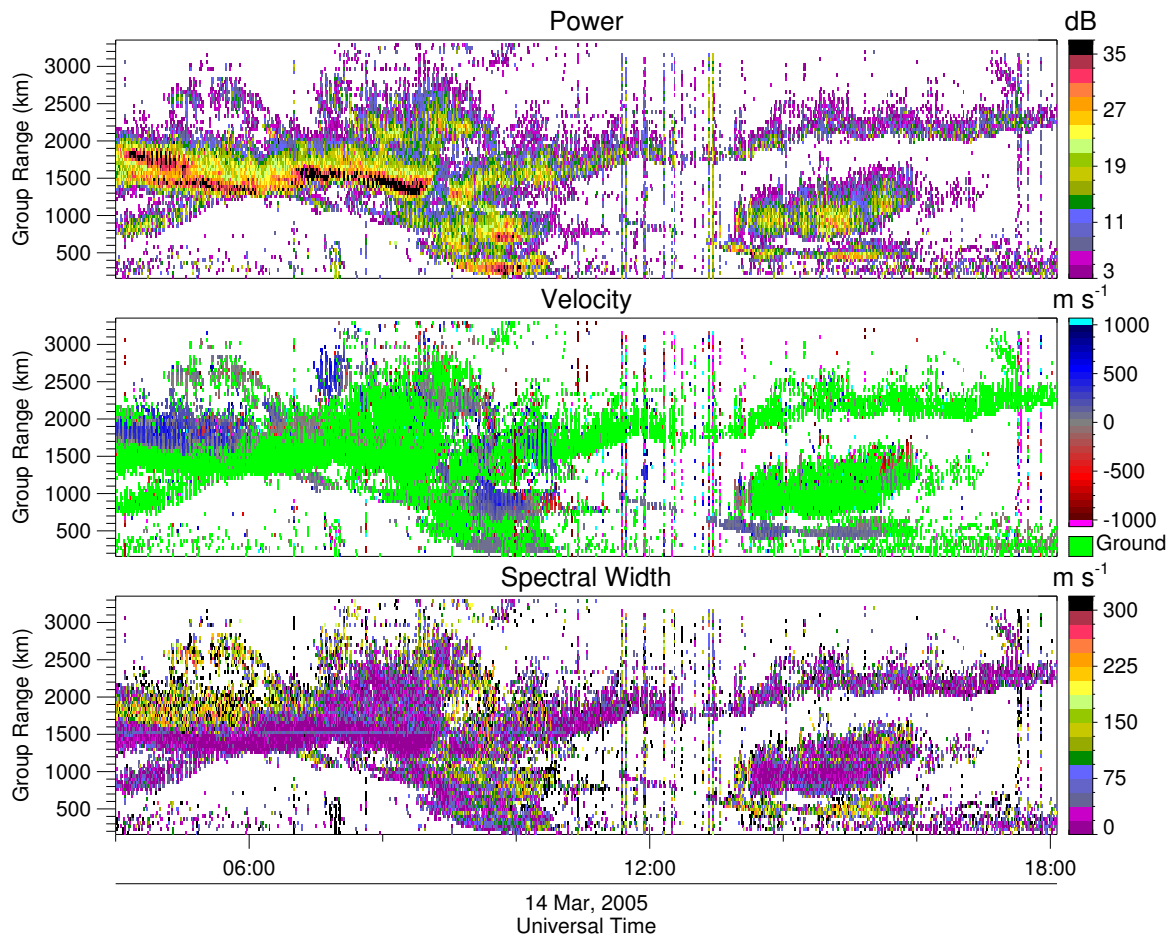
Figure 3.1: The summary plot for beam 8 of the Macquarie Island phasing box test campaign clearly shows banding indicating an alternating field of view.

From Figure 3.2 we can conclude that the Macquarie Island phasing box is working and providing the desired amount of field of view rotation.
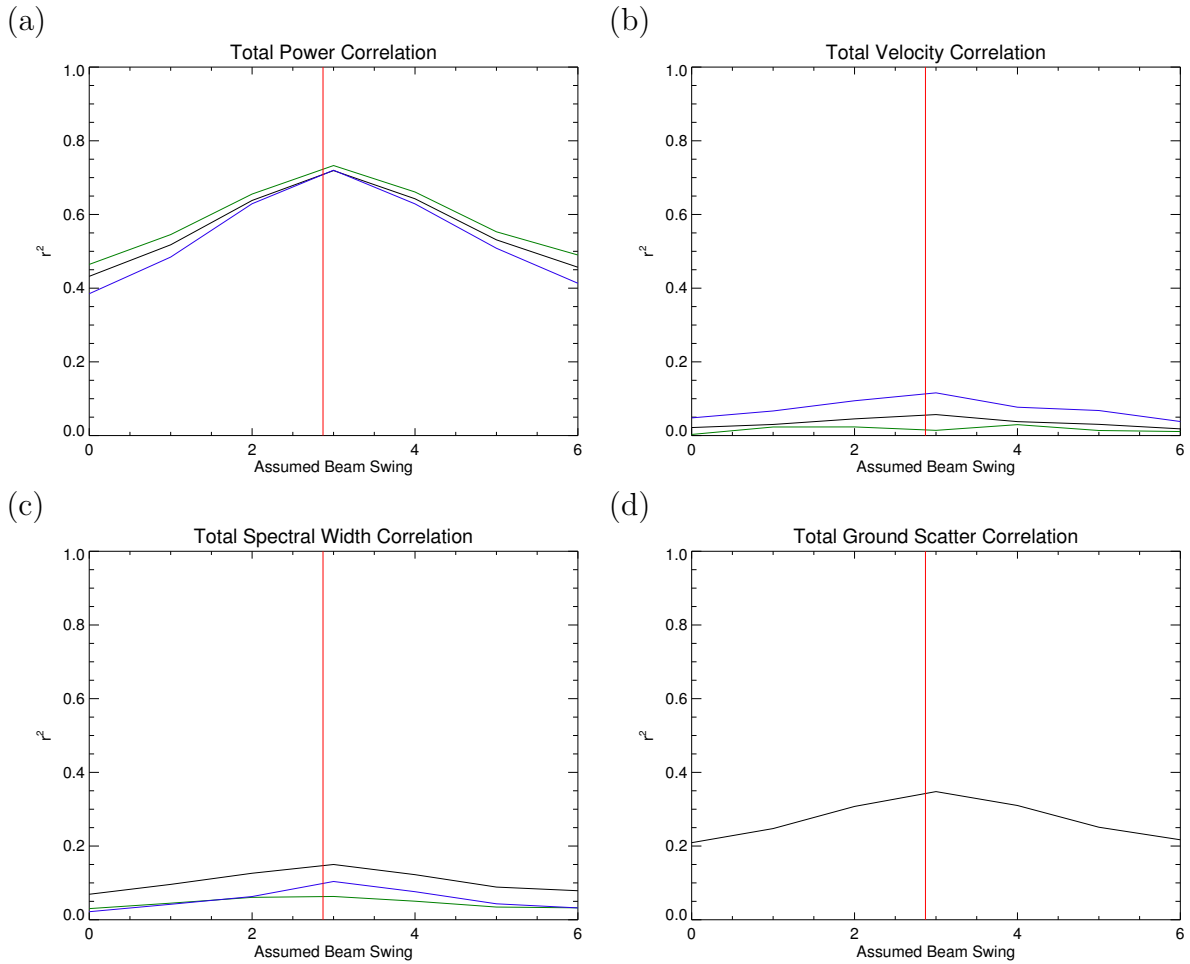
(a)

(b)

(c)

(d)

Figure 3.2: The black lines are the correlation coefficients where there was a point in both sets and with no discrimination between ionospheric or ground scatter, the blue lines are the correlation coefficients where both data sets are ionospheric scatter and the green lines are the correlation coefficients where both data sets are ground scatter. The red vertical line is the rotation that the phasing box was designed to provide

3.2 Testing the HAARP Phasing Box

A campaign was run on the Bruny Island radar to test the HAARP Phasing Box on the 23th and 24th of August, 2005. The `pbtest` program was developed for this campaign. Using `pbtest` allowed the test program to run for a full two days and so collect more data for analysis.

The summary plots for this campaign also showed strong banding on all beams. The summary plot for beam 0 is shown in Figure 3.3.
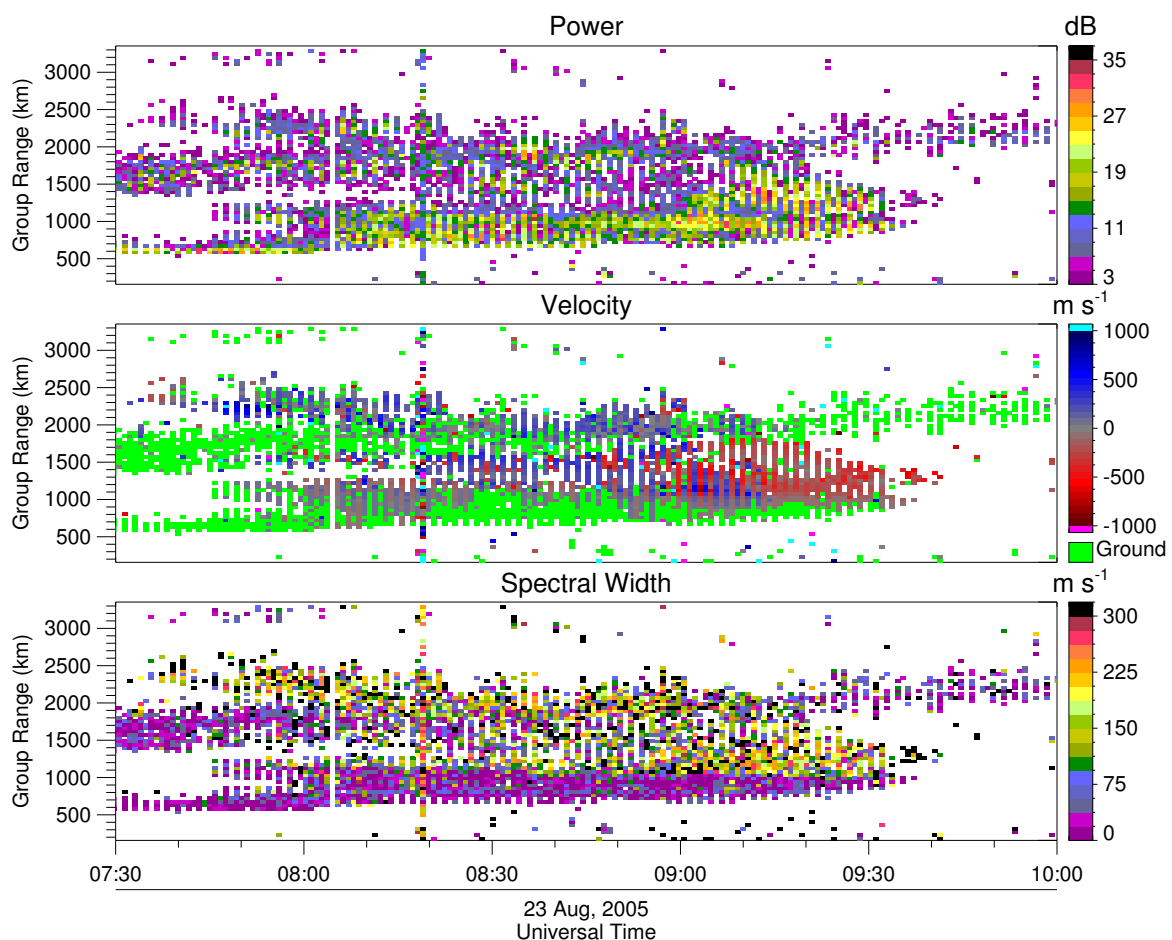

Figure 3.3: This summary plot enlargement for beam 0 of the HAARP phasing box test campaign shows the same banding that is evidence of an alternating field of view.

A correlation analysis was run using `testphasingbox` but did not appear to show a clear peak where one was expected. This could be due to the very large amount of field

of view rotation (28.5°) needed to place a beam through the HAARP conjugate point but will need to be looked at in further detail or another method used to determine the amount of field of view rotation.

4 Dual Radar Measurements Over MQI

The Macquarie Island phasing box was used to run a number of campaigns to collect data with the phasing box in use. These campaigns are listed in Table 4.1. For all

Start Time	End Time	Scan Mode	Status
2005-04-01 18:00	2005-04-08 12:00	`fast_scan`	Successful
2005-04-11 18:00	2005-04-13 06:00	`fast_scan`	Successful, Further analysed
2005-05-05 12:00	2005-05-09 06:00	`fast_scan`	Failed
2005-05-24 00:00	2005-05-26 00:00	`fast_scan`	Successful
2005-05-27 00:00	2005-05-28 06:00	`fast_scan`	Failed
2005-06-05 00:00	2005-06-09 00:00	`fast_scan`	Successful
2005-07-07 18:00	2005-07-12 00:00	`trident`	Successful
2005-07-13 00:00	2005-07-16 00:00	`trident`	Successful

Table 4.1: Campaigns run with the Macquarie Island phasing box. The `fast_scan` program performs a full scan every minute across the entire radar field of view while the `trident` program is a 96 s full scan with 3 s integration time which produces very high time resolution on a small number of beams by performing more integrations on those beams.

campaigns which generated data (i.e. not marked as "Failed") a summary plot was produced to determine which campaign would be worth analysing in more detail. The campaign between the 18:00 UT on the 11th of April and 06:00 UT on the 13th of April showed large amounts of daytime ionospheric scatter which usually indicates an active auroral electrojet and so was chosen to be analysed in more detail.

The daytime ionospheric scatter is visible on the Bruny Island summary plot shown in Figure 4.1. Some daytime ionospheric scatter can also be seen in the Unwin summary plot in Figure 4.2 but no where near as much due to problems with the Unwin radar.
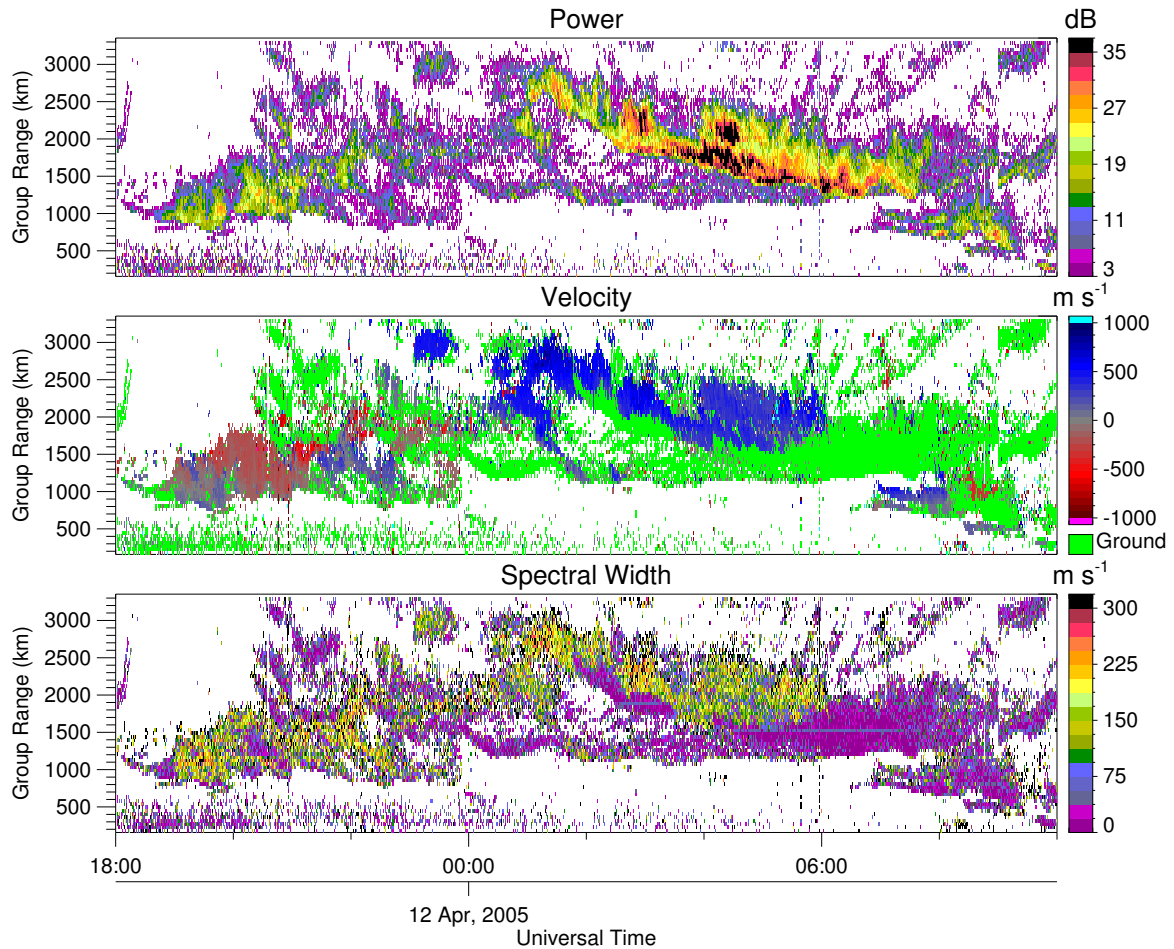
Figure 4.1: Summary plot for beam 14 (Macquarie Island beam) of the Bruny Island radar showing the daytime ionospheric scatter between 18:00 UT and 22:00 UT on the 11th of April, 2005.

Between 04:00 UT and 06:00 UT on the 12th of April there was an unusual feature in the Unwin data at a range of about 450 km and greater which might be caused by sporadic E or a meteor trail, but there is another trace slightly further away which approaches it and which may be related. As of yet this feature is not understood and it is quite possible the merging of the two traces is just a coincidence.

The measurements made during this campaign were mapped to a common grid and combined to analyse the two-dimensional convection pattern. During this analysis three types of vectors were used: the raw line of sight vectors (Figure 4.3) measured by each radar, the merged vectors (Figure 4.4) created when two raw vectors in a grid cell
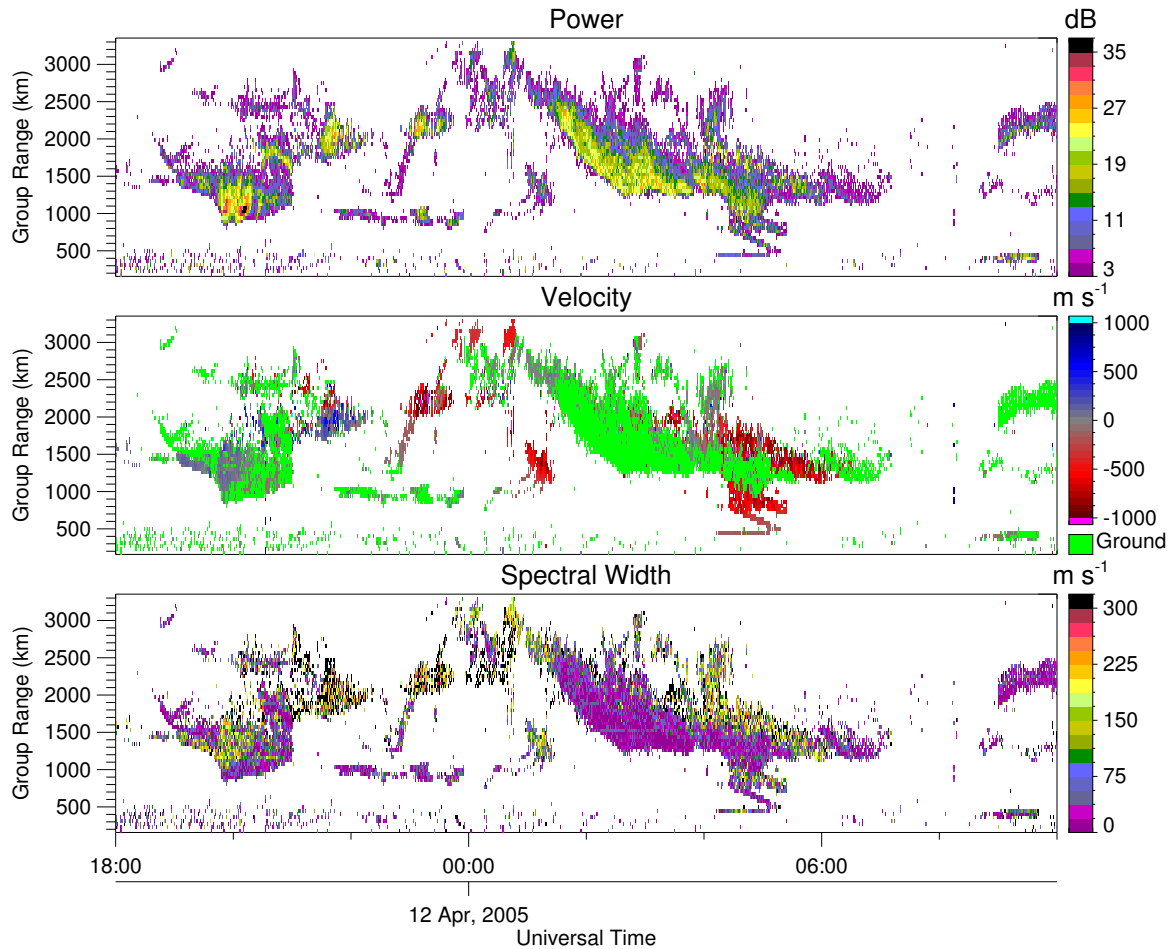
Figure 4.2: Summary plot for beam 12 (Macquarie Island beam) of the Unwin radar showing less scatter than the Bruny Island radar.

are combined and the fitted vectors (Figure 4.5) created by the map potential model discussed in §1.2.

Comparing Figures 4.3 and 4.4 it is clearly seen that only a fraction of the measurements made by each radar could be combined into a merged vector despite there being abundant line of sight vectors recorded by the Bruny Island radar.

The map potential model on the other hand, allows for the fitting of velocity vectors and the ionospheric electric potential using every line of sight velocity vector. The details of the map potential model were discussed in §1.2.

The map potential model results for 21:50 UT are shown in Figure 4.5. We can see a two convection cell pattern over the pole and what may be a new convection cell in the pre-noon sector of the sub-auroral ionosphere.
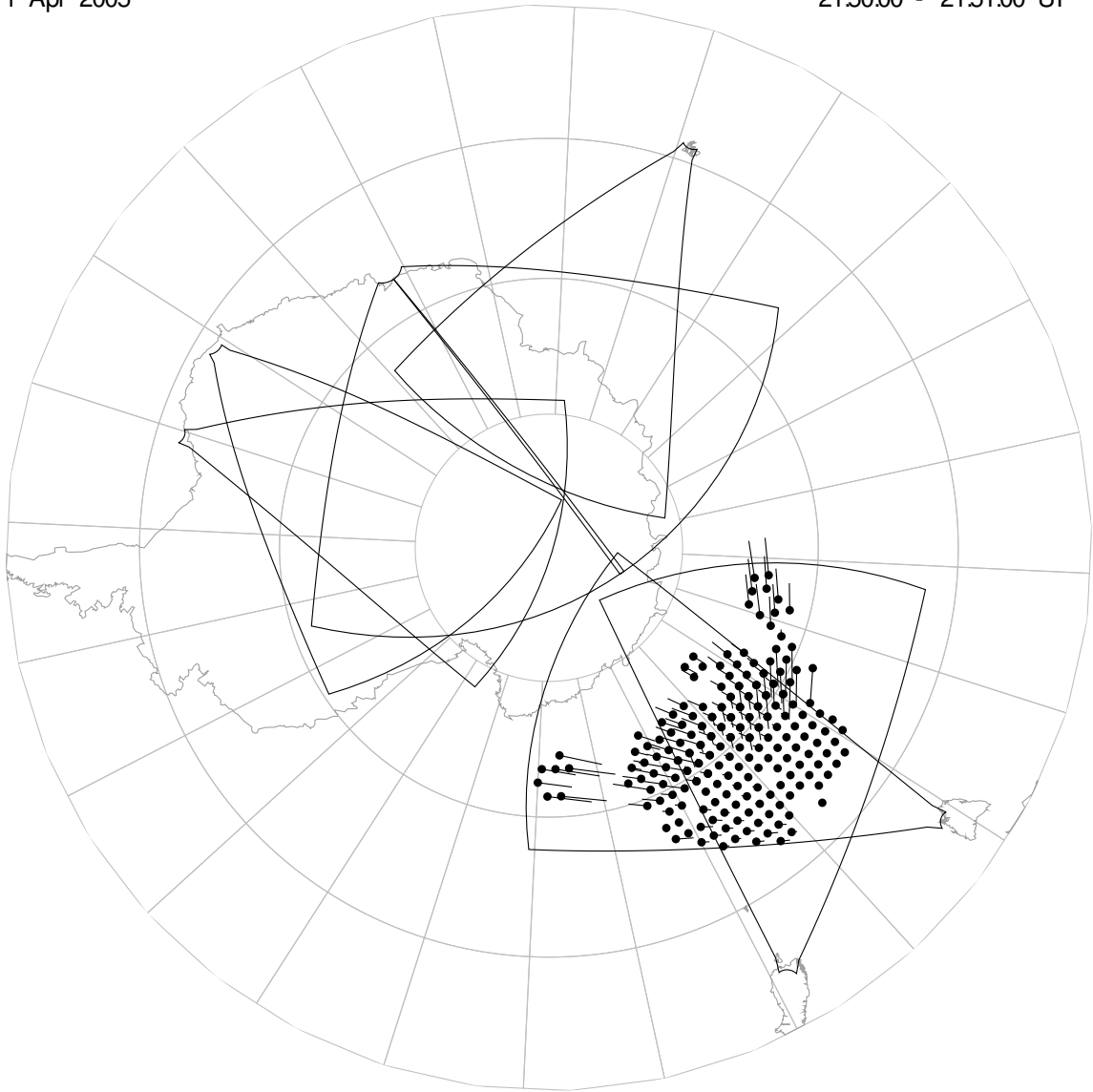
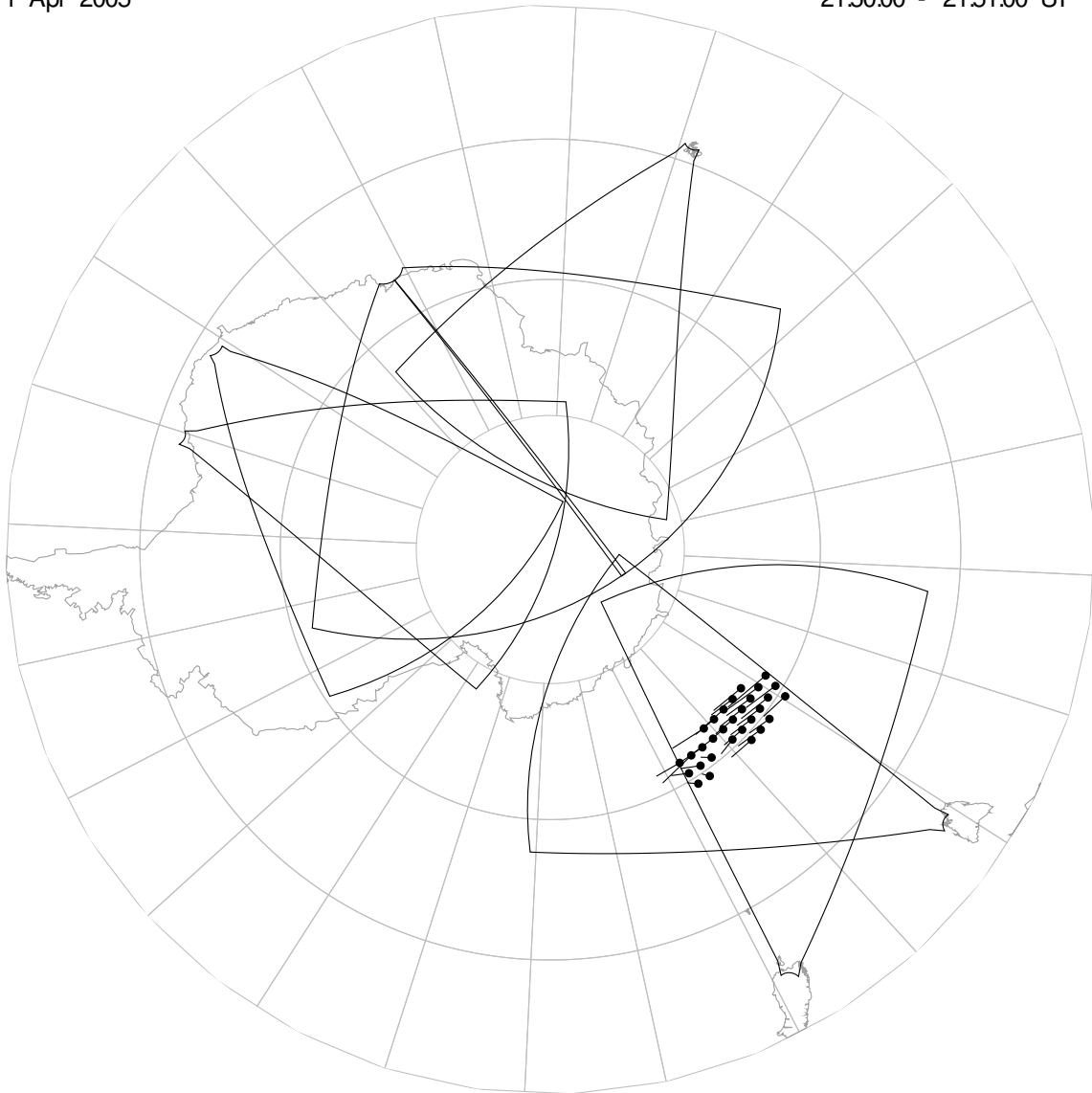Figure 4.3: The raw line of sight vectors recorded by both radars.

Figure 4.4: The merged vectors created by combining line of sight vectors in the same
grid cell. Note the lack of coverage due to most of grid cells only having data
recorded by one radar.

order=4
lat. bnd.=-50
err wt/norm mod wt
map_fit 1.09

$\chi^2/1082=0.7$
$\chi^2/209=4$

APL MODEL
4<BT<6
Bz-

Figure 4.5: The map potential model showing fitted velocity vectors over the entire region where line of sight vectors were obtained and the fitted electric isopotential lines, the accuracy of which is doubtful where no data existed to constrain the fit. Note the convection cell close in to both radars which may be a new feature.

5 HAARP Conjugacy Experiment

From the 00:00 UT on the 21st of August, 2005 to 00:00 UT on the 23rd of August, 2005 the HAARP phasing box was used to rotate the field of view of the Bruny Island radar to look at the HAARP conjugate point.

The `cont_scan` program was run with a 5 beam scan centered around the predicted HAARP conjugate point and with 3 s integration time giving a full scan every 15 s since the wait for minute boundary was removed from `cont_scan`.

The operating frequency of the radar was adjusted interactively but tended to be about 14 MHz in the day and about 9 MHz at night. Whilst the use of 14 MHz in the day resulted in large sidelobes this was required to be able to detect scatter at long ranges during the day and any effect at the approximate range of the HAARP conjugate point that is correlated with activity at HAARP could be assumed to come from the mainlobe and not a sidelobe.

The experimental results are shown in Figure 5.1. There was no clear evidence of an inter-hemispheric effect although there was an unusual increase in the signal to noise ratio and range width over which the radar obtained an echo (enlarged in Figure 5.2). This is believed to have been an instrumental effect due to the fact that the radar had been rebooted both before and after the anomalous event.
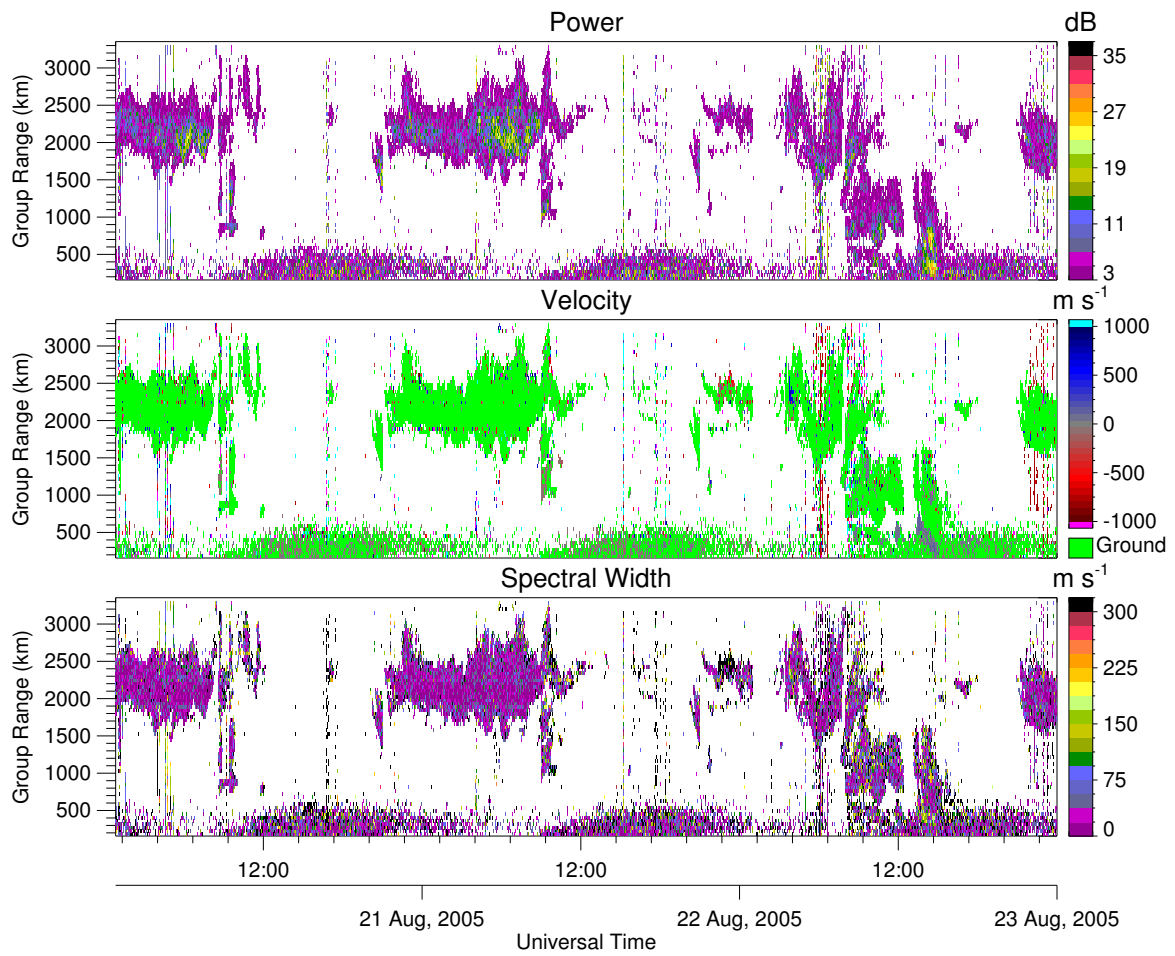
Figure 5.1: The summary plot for beam 12 of the HAARP conjugate point campaign does not show any good evidence for an inter-hemispheric effect.
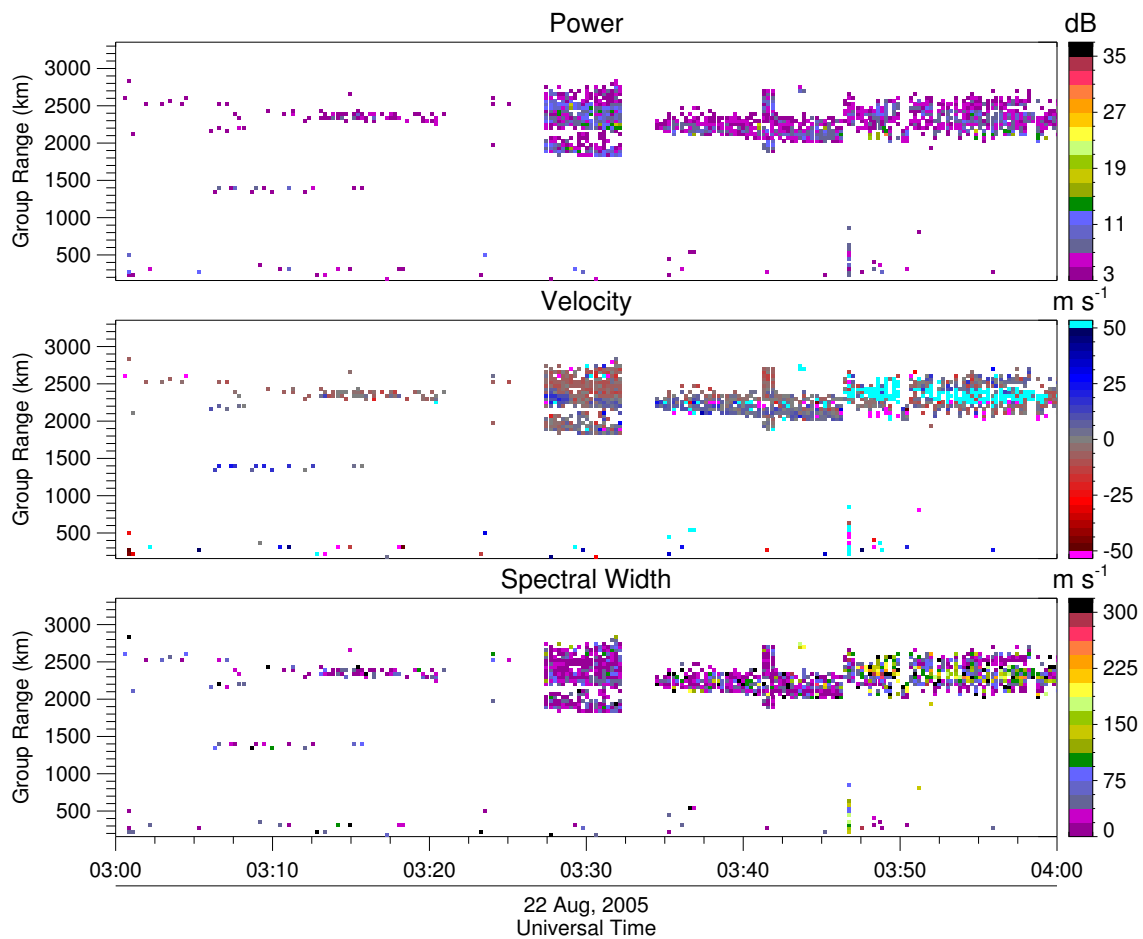
Figure 5.2: The anomalous increase in power and range width along beam 12 can be seen clearly in this enlargement. Note the lack of data for a short period both before and after the anomalous event when the radar was rebooted. This same effect was visible on all beams.

6 Summary

The Macquarie Island phasing box is working and providing the intended 9.3° field of view rotation.

The HAARP conjugate point phasing box is providing a change of the field of view but the change being provided has not yet been determined. This will have to be analysed in further detail.

The map potential model is working on TIGER data and may have discovered a new convection cell in the morning sector sub-auroral ionosphere.

The attempt to detect an inter-hemispheric effect at the HAARP conjugate point does not appear to have found any effect however this experiment is likely to be subject to considerable natural variability.

6.1 Future Experiments

The HAARP phasing box test data will need to be analysed in more detail to determine if it is actually rotating the field of view in the intended manner before there is confidence in HAARP conjugate point campaigns.

The event analysed with map potential will need to be examined in further detail, particularly the possible new convection cell in the context of coincident spacecraft results and ground based magnetometer results. Re-running the map potential model with data from the Antarctic radars will also better constrain the fitted electric isopotentials.

The additional capabilities provided by the Macquarie Island phasing box will allow for improved comparisons between measurements made by instruments on Macquarie Island with measurements made by the TIGER radars. This may improve studies of the effects of Travelling Ionospheric Disturbances and Ultra Low Frequency waves in the ionosphere. Placing Macquarie Island in the field of view of both radars will also provide a zero velocity Doppler target to improve atmospheric gravity wave studies and sea state studies.

The experiment to detect inter-hemispheric effects due to HAARP will need to be repeated many times due to the natural variability inherent in the magnetosphere-ionosphere system. If an inter-hemispheric effect can be detected it will open up the possibility of controlled experiments in magnetic conjugacy including measuring the transfer function for magnetsohpere-ionosphere coupling.

The presence of high powered HF radio transmitters including those used by radio stations should be considered when choosing the field of view of a new SuperDARN radar.

The new phasing box that is being completed for the Unwin radar will allow for comparisons between E and F region scatter on the same field lines. Using both the new E-F Region phasing box and the Macquarie Island phasing box together will allow for measurements at even lower magnetic latitudes to be taken which will extend the map potential model even further equatorward.

7 Bibliography

[1] Wallace H. Campbell.
Introduction to Geomagnetic Fields.
Cambridge University Press, second edition, 2003.

[2] David Smith – Australian Antarctic Division.
Personal Communication.

[3] Kenneth Davis.
Ionospheric Radio, volume 31 of *IEE Electromagnetic Waves*.
Peter Peregrinus Ltd. on behalf of the Institution of Electrical Engineers, 1990.

[4] Australian Antarctic Division.
Macquarie Island.
World Wide Web.
`http://www.aad.gov.au/default.asp?casid=7151`
    Accessed 2005-08-31
    Last updated 2004-07-19.

[5] P. L. Dyson, J. C. Devlin, M. L. Parkinson, and J. S. Whittington.
The Tasman International Geospace Environment Radar (TIGER) — Current Development and Future Plans.
IEEE Proceedings of the International Conference on Radar, pages 282–287, 2003.

[6] R. A. Greenwald, K. B. Baker, J. R. Dedeney, M. Pinnock, T. B. Jones, E. C. Thomas, J.-P. Villain, J.-C. Cerisher, C. Senior, C. Hanuise, R. D. Hunsucker, G. Sofko, J. Koehler, E. Nielsen, R. Pellinen, A. D. M. Walker, N. Sato, and H. Yamagishi.
DARN/SUPERDARN. A Global View of the Dynamics of High-Lattitude Convection.
Space Science Reviews, 71(1–4):761–796, February 1995.

[7] Todd R. Pedersen and Elizabeth A. Gerken.
Creation of visible artificial optical emissions in the aurora by high-power radio waves.
Nature, 433(7025):498–500, February 2005.

[8] R. A. Greenwald, K. B. Baker, R. A. Hutchins and C. Hanuise.
An HF phased-array radar for studying small-scale structure in the high-lattitude ionosphere.
Radio Science, 20(1):63–79, 1985.

[9] R. S. Dhilon, T. R. Robinson and D. M. Wright.
Radar ACFs and turbulence characteristics from artificially generated field-aligned
irregularities.
Geophysical Research Letters, 27(17):1 830, September 2002.

[10] Ray Morris – Australian Antartic Division.
Personal Communication.

[11] Raymond A. Greenwald.
Space weather, superdarn and the tasmanian tiger.
Australian Journal of Physics, 50(4):773–792, 1997.

[12] J. M. Ruohoniemi and K. B. Baker.
Large-scale imaging of high-lattitude convection with Super Dual Auroral Radar
Network HF radar observations.
Journal of Geophysical Research, 103(A9):20 797–20 811, September 1998.

[13] J. M. Ruohoniemi, R. A. Greenwald, K. B. Baker, J.-P. Villain, C. Hanuise, and
J. Kelly.
Mapping High-Lattitude Plasma Convection With Coherent HF Radars.
Journal of Geophysical Research, 94(A10):13 463–13 477, October 1989.

[14] T. Sergienko, I. Kornilov, E. Belove, T. Turunen, and J. Manninen.
Optical effects in the aurora caused by ionospheric HF heating.
Journal of Atmospheric and Solar-Terrestrial Physics, 59(18):2 401–2 407, December 1997.

[15] A. J. Stocker, T. R. Robinson, T. B. Jones, and P. Stubbe.
The effect of artificial modification in the E region on HF ray propagation.
Journal of Atmosphic and Solar-Terrestrial Phyics, 59(18):2 435–2 446, December
1997.

[16] Peter Stubbe.
Review of ionospheric modification experiments at Tromsø.
Journal of Atmospheric & Terrestrial Physics, 58(1–4):349–368, 1996.

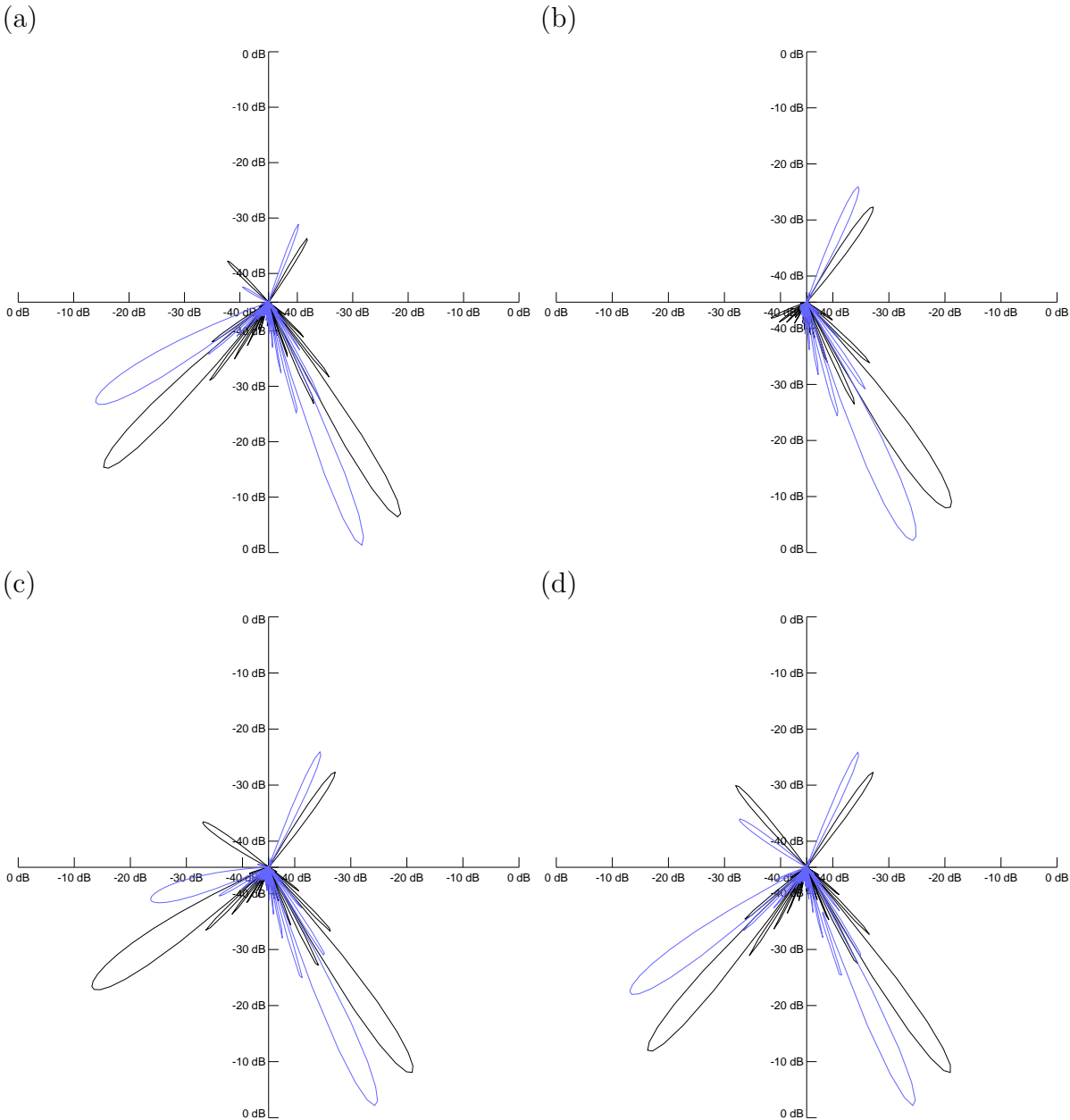# A Antenna Patterns

(a)

(b)

(c)

(d)

Figure A.1: Radiation Patterns with the Macquarie Island phasing box in use (black) and not in use (blue). (a) is the radiation pattern for beam 14 (Macquarie Island beam) at 16 MHz. (b) is the radiation pattern for beam 15 (Most degraded beam) at 12 MHz, (c) is the radiation pattern for beam 15 at 14 MHz and (d) is the radiation pattern for beam 15 at 16 MHz.
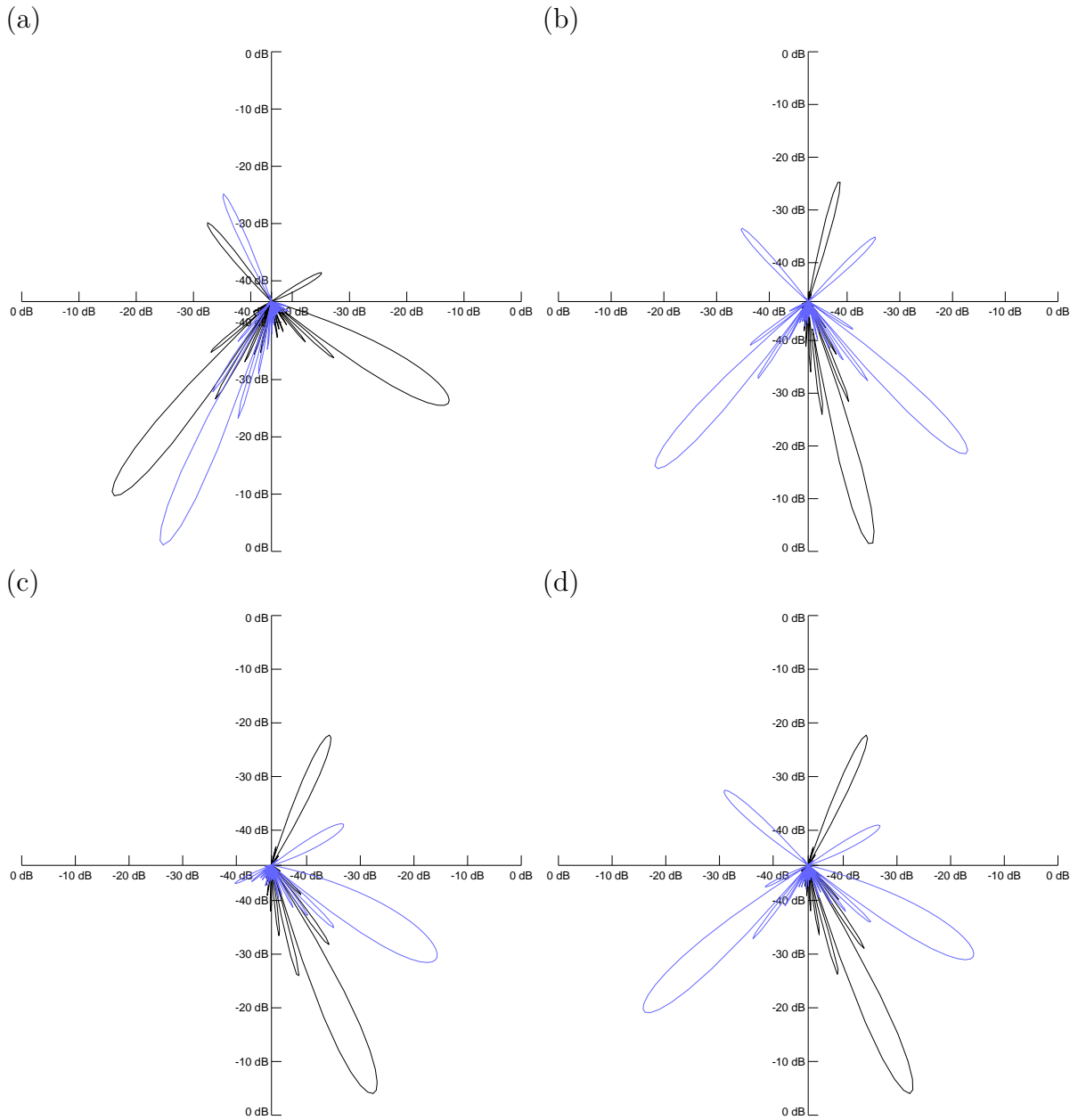
(a)

(b)

(c)

(d)

Figure A.2: Additional radiation patterns. (a) is the radiation pattern for beam 0 with the E-F region phasing box in use (black) and not in use (blue) at 13 MHz. (b) is the radiation pattern for beam 12 (through HAARP conjugate point) with the HAARP phasing box in use (blue) and not in use (black) at 14 MHz. (c) is the radiation pattern for beam 15 (most degraded beam) with the HAARP phasing box in use (blue) and not in use (black) at 10 MHz and (d) is the radiation pattern for beam 15 with the HAARP phasing box in use (blue) and not in use (black) at 12 MHz.

B Phasing Box Time Delays

Antenna	Ideal Delay	Rounded	1st	2nd	3rd	Total	Error
0	0.0	0				0	0.0
1	8.2	7.5	5	2.5		7.5	-0.7
2	16.4	17.5	15	2.5		17.5	1.1
3	24.6	25	25			25	0.4
4	32.8	32.5	30	2.5		32.5	-0.3
5	41.0	40	40			40	-1.0
6	49.3	50	50			50	0.7
7	57.5	57.5	50	5	2.5	57.5	0.0
8	65.7	65	60	5		65	-0.7
9	73.9	75	60	15		75	1.1
10	82.1	82.5	80	2.5		82.5	0.4
11	90.3	90	80	10		90	-0.3
12	98.5	100	100			100	1.5
13	106.7	107.5	100	5	2.5	107.5	0.8
14	114.9	115	100	15		115	0.1
15	123.1	125	100	25		125	1.9

Table B.1: Ideal time delays to place beam 14 above Macquarie Island and the time delays actually used (in ns).

Antenna	Ideal Delay	Rounded	1st	2nd	3rd	4th	Total	Error
0	0.0	0					0	0.0
1	24.3	25	25				25	0.7
2	48.5	47.5	40	5	2.5		47.5	-1.0
3	72.8	72.5	60	10	2.5		72.5	-0.3
4	97.0	97.5	80	15	2.5		97.5	0.5
5	121.3	122.5	100	20	2.5		122.5	1.2
6	145.5	145	100	40	5		145	-0.5
7	169.8	170	100	60	10		170	0.2
8	194.1	195	100	80	15		195	0.9
9	218.3	217.5	100	100	15	2.5	217.5	-0.8
10	242.6	242.5	100	100	40	2.5	242.5	-0.1
11	266.8	267.5	100	100	60	7.5	267.5	0.7
12	291.1	290	100	100	80	10	290	-1.1
13	315.3	315	100	100	100	15	315	-0.3
14	339.6	340	100	100	100	40	340	0.4
15	363.8	365	100	100	100	60	360	-3.8

Table B.2: Ideal time delays to reach the HAARP conjugate point and the time delays actually used (in ns).

Antenna	Ideal Delay	Rounded	1st	2nd	3rd	Total	Error
0	171.0	170	100	60	10	170	-1.0
1	159.6	160	100	60		160	0.4
2	148.2	147.5	100	50		150	1.8
3	136.8	137.5	100	25	10	135	-1.8
4	125.4	125	100	25		125	-0.4
5	114.0	115	100	15		115	1.0
6	102.6	102.5	100	2.5		102.5	-0.1
7	91.2	90	80	10		90	-1.2
8	79.8	80	80			80	0.2
9	68.4	67.5	60	5	2.5	67.5	-0.9
10	57.0	57.5	50	5	2.5	57.5	0.5
11	45.6	45	40	5		45	-0.6
12	34.2	35	30	5		35	0.8
13	22.8	22.5	20	2.5		22.5	-0.3
14	11.4	12.5	10	2.5		12.5	1.1
15	0.0	0				0	0.0

Table B.3: Ideal time delays to rotate Unwin to look at F Region scatter above Bruny Island E Region scatter and the time delays actually used (in ns).
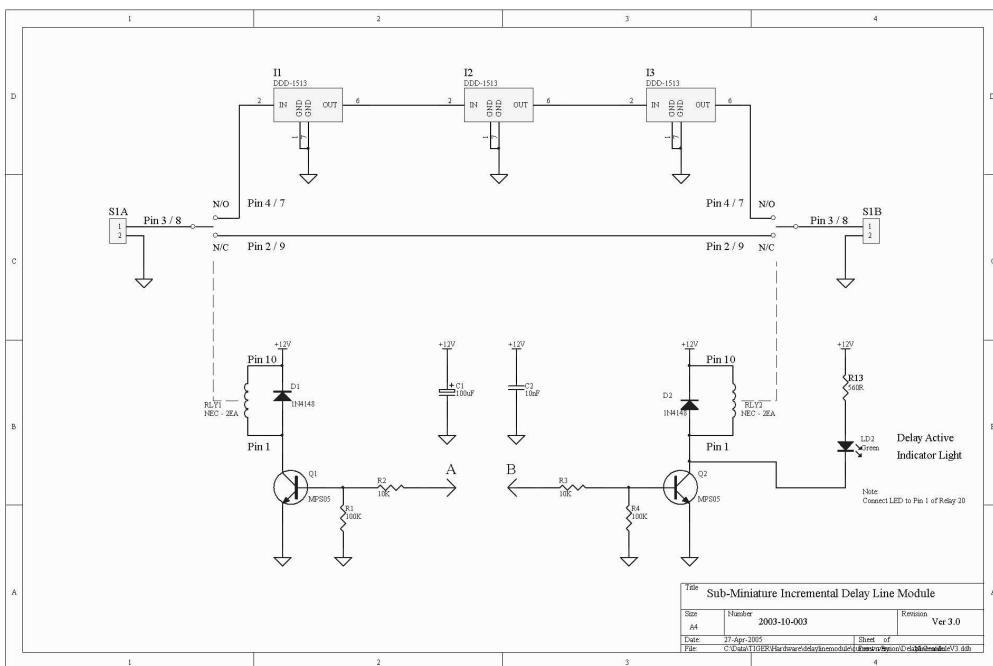
C Phasing Box Circuit Diagrams

Figure C.1: Circuit diagram of one of the 20 paths a signal passes through the phasing box. The top shows that with the relay on the signal passes through the three delays lines shown and bypasses them with the relay set to off. The bottom is the relay control circuitry.
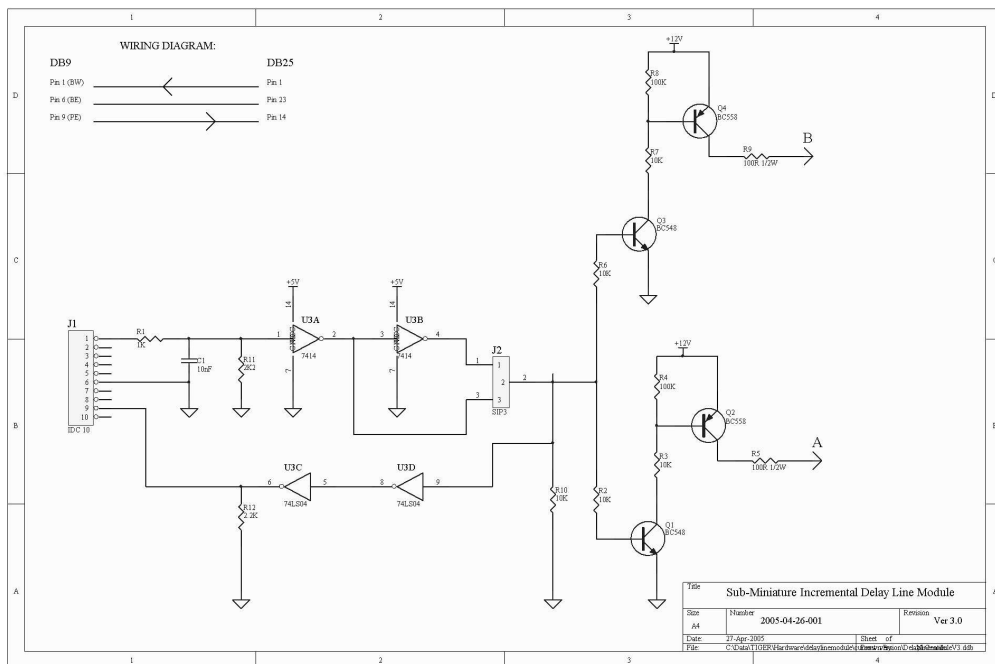
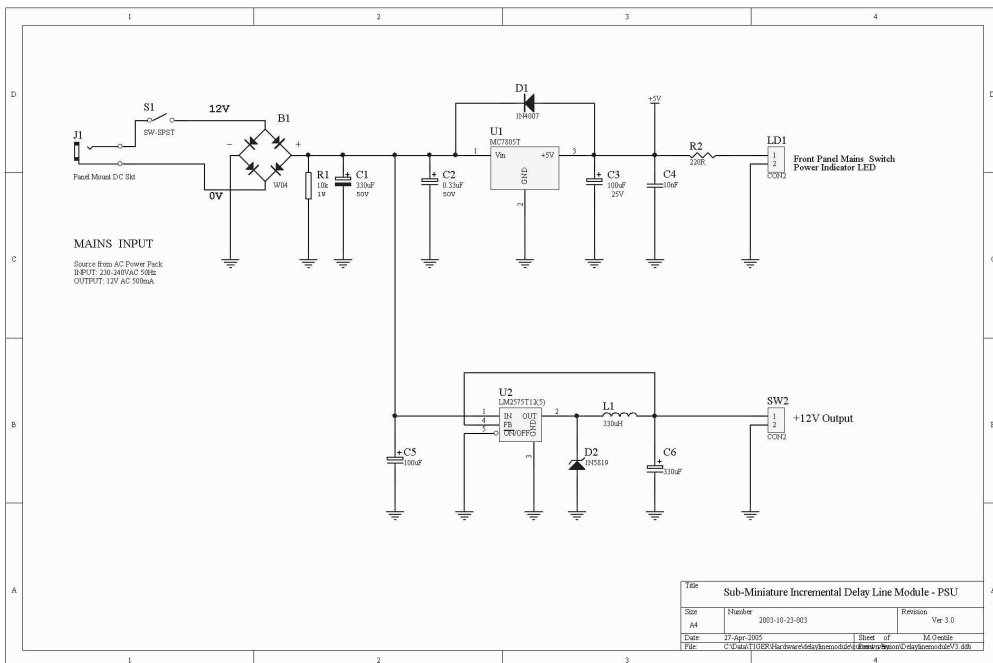Figure C.2: Circuit diagram of the control circuit that receives commands from the BAS-box to turn the phasing box on and off and reads the current status of the phasing box back to the BASbox.

Figure C.3: Circuit diagram of the power supply unit for a phasing box.
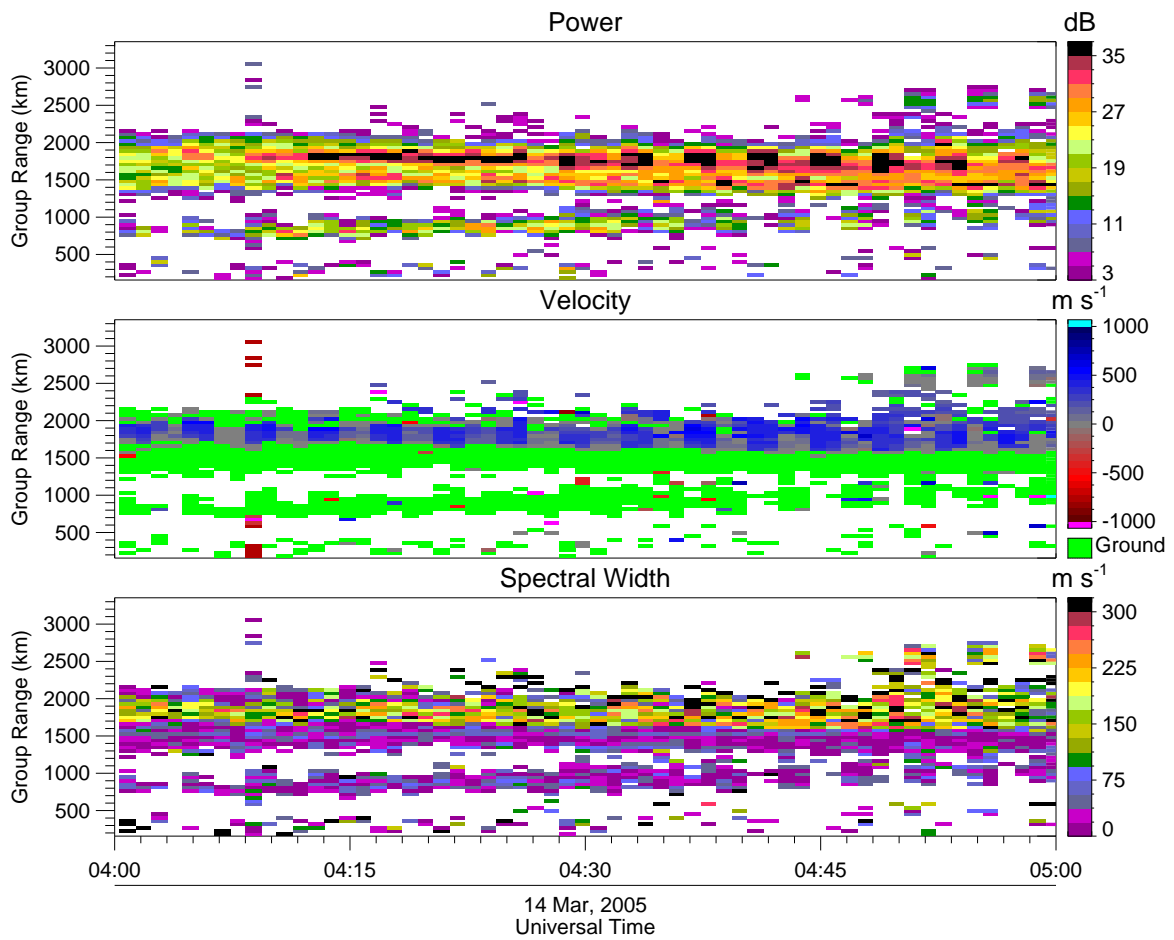
D Summary Plots

Figure D.1: Enlargement of Macquarie Island phasing box test for beam 8 between 4:00 UT and 5:00 UT.
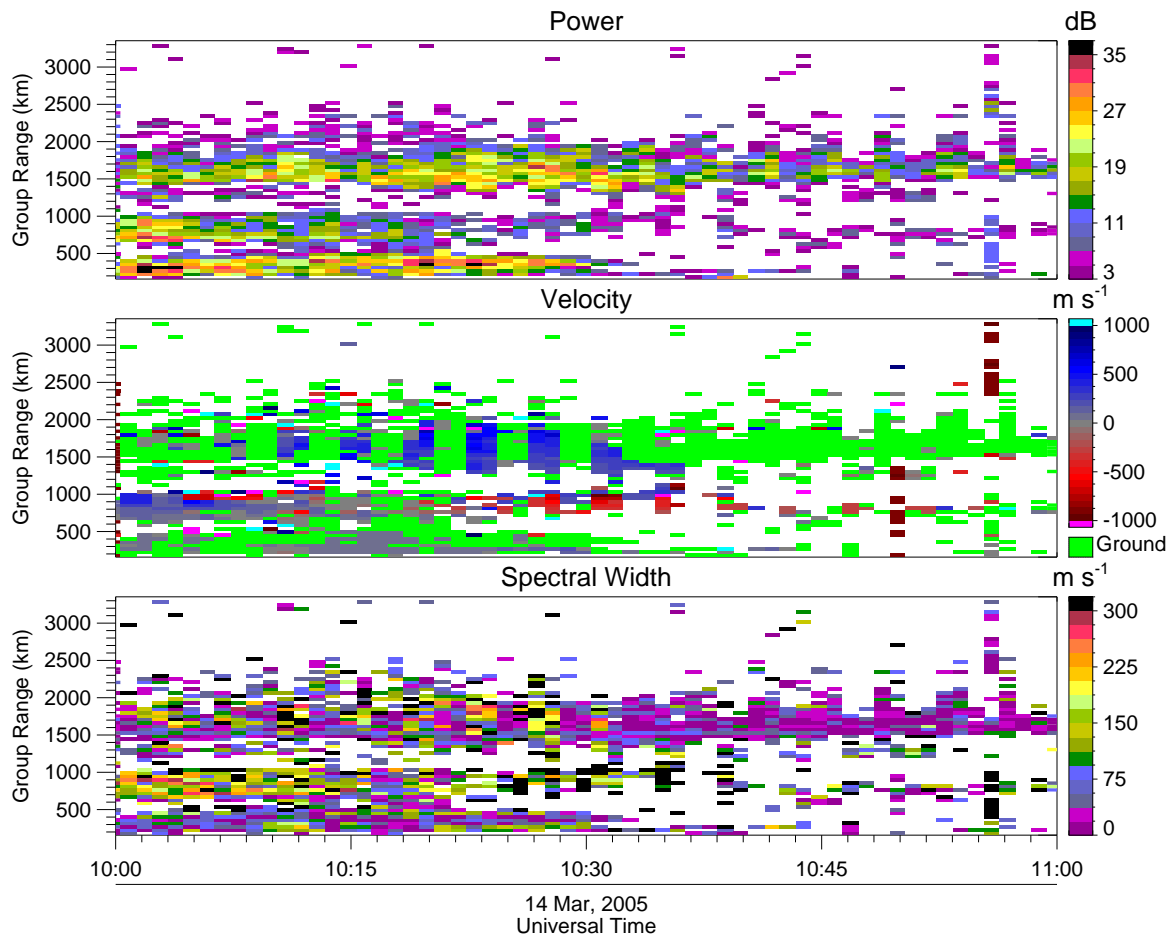
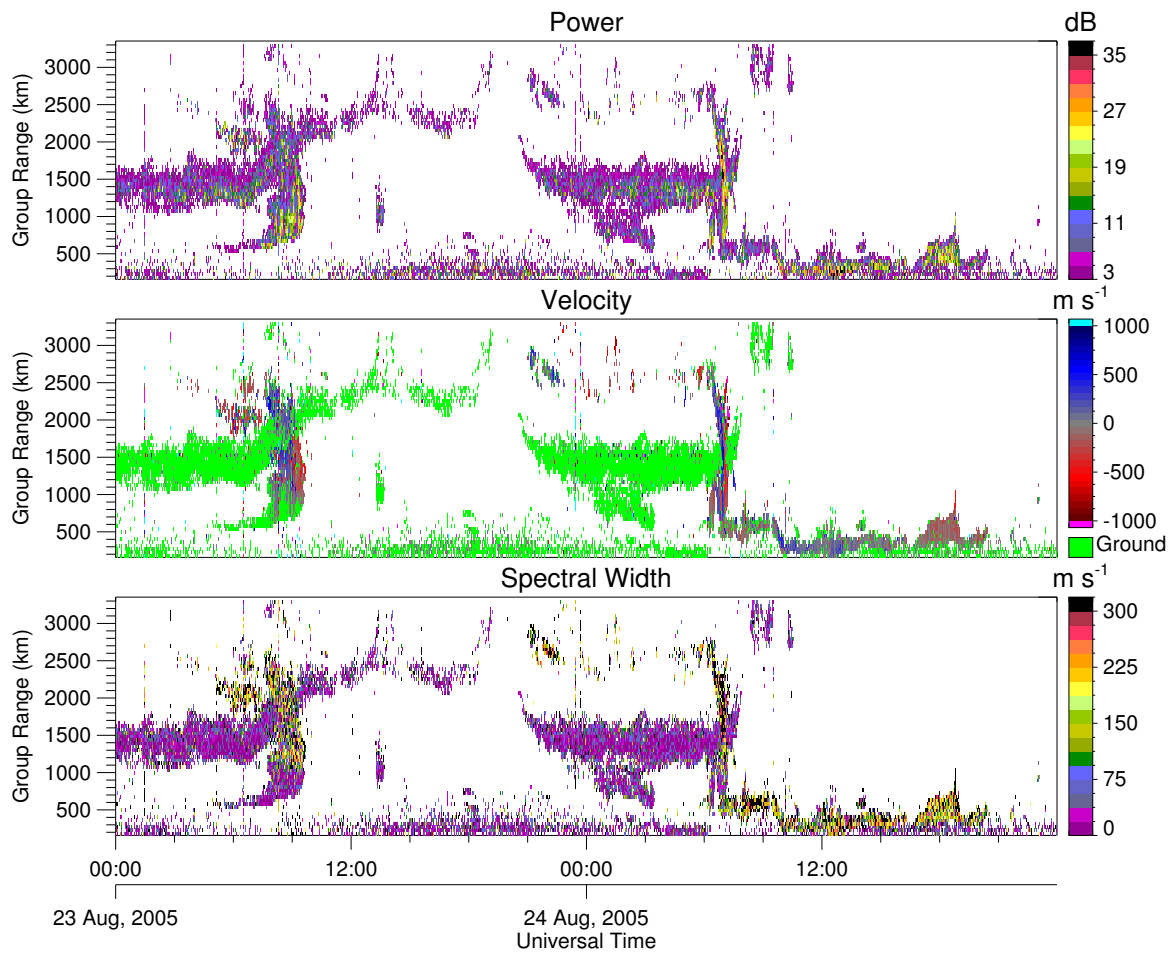Figure D.2: Enlargment of Macquarie Island phasing box test for beam 8 between 10:00 UT and 11:00 UT.

Figure D.3: Summary plot of entire HAARP phasing box test campaign for beam 0.